SANDIA REPORT
SAND2005-5748
Unlimited Release
Printed November 2006

Fabrication, Testing, and Analysis of Anisotropic Carbon/Glass Hybrid Composites
Volume 1: Technical Report

Thomas M. Hermann, James E. Locke, and Kyle K. Wetzel

Prepared by
Sandia National Laboratories
Albuquerque, New Mexico 87185 and Livermore, California 94550

Sandia is a multiprogram laboratory operated by Sandia Corporation,
a Lockheed Martin Company, for the United States Department of Energy's
National Nuclear Security Administration under Contract DE-AC04-94AL85000.

Approved for public release; further dissemination unlimited.

Issued by Sandia National Laboratories, operated for the United States Department of Energy by Sandia Corporation.

NOTICE: This report was prepared as an account of work sponsored by an agency of the United States Government. Neither the United States Government, nor any agency thereof, nor any of their employees, nor any of their contractors, subcontractors, or their employees, make any warranty, express or implied, or assume any legal liability or responsibility for the accuracy, completeness, or usefulness of any information, apparatus, product, or process disclosed, or represent that its use would not infringe privately owned rights. Reference herein to any specific commercial product, process, or service by trade name, trademark, manufacturer, or otherwise, does not necessarily constitute or imply its endorsement, recommendation, or favoring by the United States Government, any agency thereof, or any of their contractors or subcontractors. The views and opinions expressed herein do not necessarily state or reflect those of the United States Government, any agency thereof, or any of their contractors.

Printed in the United States of America. This report has been reproduced directly from the best available copy.

Available to DOE and DOE contractors from
U.S. Department of Energy
Office of Scientific and Technical Information
P.O. Box 62
Oak Ridge, TN 37831

Telephone: (865) 576-8401
Facsimile: (865) 576-5728
E-Mail: reports@adonis.osti.gov
Online ordering: http://www.osti.gov/bridge

Available to the public from
U.S. Department of Commerce
National Technical Information Service
5285 Port Royal Rd.
Springfield, VA 22161

Telephone: (800) 553-6847
Facsimile: (703) 605-6900
E-Mail: orders@ntis.fedworld.gov
Online order: http://www.ntis.gov/help/ordermethods.asp?loc=7-4-0#online

COPYRIGHT NOTICE

Copyright © 2005 Wetzel Engineering, Inc., and Wichita State University

The U.S. Government retains certain interests in the copyrights to this document as per the terms of Grant DE-FG02-03ER86175 by and between Wetzel Engineering, Inc., and the United States Department of Energy.

All Other Rights Reserved by
Wetzel Engineering, Inc., and Wichita State University

The contents of this document, including both text and graphics, may be reproduced without royalty for educational and nonprofit research purposes only, provided that full citation of the current document is noted, including all authors and affiliations. Reproduction for any for-profit or commercial purpose is strictly prohibited without the express and written permission of Wetzel Engineering, Inc.

SAND2005-5748
Unlimited Release
Printed November 2006

FABRICATION, TESTING AND ANALYSIS OF ANISOTROPIC, CARBON/GLASS HYBRID COMPOSITES

Thomas M. Hermann and James E. Locke
National Institute for Aviation Research
Wichita State University
Wichita, Kansas 67260

Kyle K. Wetzel
Wetzel Engineering, Inc.
Lawrence, Kansas 66046

Abstract

Anisotropic carbon/glass hybrid composite laminates have been fabricated, tested, and analyzed. The laminates have been fabricated using vacuum-assisted resin transfer molding (VARTM). Five fiber complexes and a two-part epoxy resin system have been used in the study to fabricate panels of twenty different laminate constructions. These panels have been subjected to physical testing to measure density, fiber volume fraction, and void fraction. Coupons machined from these panels have also been subjected to mechanical testing to measure elastic properties and strength of the laminates using tensile, compressive, transverse tensile, and in-plane shear tests. Interlaminar shear strength has also been measured. Out-of-plane displacement, axial strain, transverse strain, and in-plane shear strain have also been measured using photogrammetry data obtained during edgewise compression tests.

The test data have been reduced to characterize the elastic properties and strength of the laminates. Constraints imposed by test fixtures might be expected to affect measurements of the moduli of anisotropic materials; classical lamination theory has been used to assess the magnitude of such effects and correct the experimental data for the same. The tensile moduli generally correlate well with experiment without correction and indicate that factors other than end constraints dominate. The results suggest that shear moduli of the anisotropic materials are affected by end constraints.

Classical lamination theory has also been used to characterize the level of extension-shear coupling in the anisotropic laminates. Three factors affecting the coupling have been examined: the volume fraction of unbalanced off-axis layers, the angle of the off-axis layers, and the composition of the fibers (i.e., carbon or glass) used as the axial reinforcement. The results indicate that extension/shear coupling is maximized with the least loss in axial tensile stiffness by using carbon fibers oriented 15° from the long axis for approximately two-thirds of the laminate volume (discounting skin layers), with reinforcing carbon fibers oriented axially comprising the remaining one-third of the volume.

Finite element analysis of each laminate has been performed to examine first ply failure. Three failure criteria - maximum stress, maximum strain, and Tsai-Wu - have been compared. Failure predicted by all three criteria proves generally conservative, with the stress-based criteria the most conservative. For laminates that respond nonlinearly to loading, large error is observed in the prediction of failure using maximum strain as the criterion.

This report documents the methods and results in two volumes. Volume 1 contains descriptions of the laminates, their fabrication and testing, the methods of analysis, the results, and the conclusions and recommendations. Volume 2 contains a comprehensive summary of the individual test results for all laminates.

Acknowledgments

This work has been supported by a grant from the U.S. Department of Energy via Agreement number DE-FG02-03ER86174 by and between USDOE and Wetzel Engineering, Inc. Dr. Jack Cadogan is Project Officer.

Several people at the National Institute for Aviation Research have assisted with the fabrication and testing reported here, including Drs. Yeow Ng and Brijesh Kumar, as well as Lamia Salah, Sanjay Sharma, Wadii Benjaliny, Ian Goodman, and Waruna Seneviratne.

We would like to acknowledge Chris Kissinger and Saertex USA for the donation of some of the glass materials used in the present research and for his help in sourcing appropriate fiber complexes, and Jeff Bassman of JeffCo Products, for his assistance in developing an appropriate resin system for our hybrid laminates.

Finally, we would also like to acknowledge the advice and technical expertise that has been provided in connection with this project more informally by a number of our colleagues in the wind energy industry, including Drs. Paul Veers, Tom Ashwill, and Daniel Laird of Sandia National Laboratories, Emil Moroz of Garrad Hassan America, Eric Jacobsen of GE Wind Energy, and Dr. Wendy Lin of GE Global Research.

The authors greatly appreciate all of this support.

Contents
Volume 1

List of Tables

List of Figures

Nomenclature

ϵ_{xc}	Ultimate compressive strain parallel to the fibers.
ϵ_{xt}	Ultimate tensile strain parallel to the fibers.
ϵ_{yc}	Ultimate compressive strain perpendicular to the fibers.
ϵ_{yt}	Ultimate tensile strain perpendicular to the fibers.
γ_{xy}	Ultimate in-plane shear strain.
ν_{xy}	Major Poisson's ratio.
ϕ_a	Void content.
ρ	Density.
ρ_f	Fiber density.
σ	Stress.
E_x	Modulus of elasticity parallel to the fibers.
E_y	Modulus of elasticity perpendicular to the fibers.
G_{xy}	Shear modulus in the xy plane.
S	Ultimate in-plane shear strength.
v	Deflection in the Y direction.
V_f	Fiber volume fraction.
w	Deflection in the Z direction.
$w_{,x}$	Vertical slope in the X direction,$\partial w/\partial x$.
X_c	Ultimate compressive strength parallel to the fibers.
X_t	Ultimate tensile strength parallel to the fibers.
Y_c	Ultimate compressive strength perpendicular to the fibers.
Y_t	Ultimate tensile strength perpendicular to the fibers.
CLT	Classical lamination theory.
CMM	Coordinate measuring machine.
FEA	Finite element analysis.
RTM	Resin transfer molding.
VARTM	Vacuum assisted resin transfer molding.

1. Introduction

Anisotropic carbon/glass hybrid composite laminates have been fabricated, tested and analyzed. The laminates were fabricated utilizing the vacuum assisted resin transfer molding(VARTM) technique. Five fiber complexes, listed in Table 1.1, were utilized in the study. The fabrics were supplied by Saertex USA (Mooresville, North Carolina). Four of the fabrics are presented in Figure 1.1. A two part epoxy system consisting of JeffCo Products (San Diego, California) 1401-21/16 resin and 4101-21 hardener (slow) was utilized for the matrix of the laminates. Details of the fabrication are presented in Section 2.

Twenty laminate types were manufactured for this study, listed in Table 1.2. Laminates 1, 2, 18 and 20 are each constructed of only one of the fiber complexes listed in Table1.1. Laminates 1 and 2 are pure unidirectional glass and carbon, respectively, while Laminates 18 and 20 are the two biaxial ($\pm 45^\circ$) glass complexes. Testing of these laminates allows measurement of the constitutive properties of the fiber complexes used to construct all the remaining laminates. Laminates 3 and 4 differ from 1 and 2 by the addition of biaxial glass skin layers to the outside of the unidirectional glass or carbon. This construction is representative of industrial composite spar cap (flange) fabrication. Laminates 5, 7 and 8 modify Laminate 4 by rotating increasing fractions of the unidirectional carbon fibers to a 20° orientation relative to the long axis of the coupons. Laminates 6 and 9 modify Laminate 3 by doing the same to the unidirectional glass fibers. The testing of these laminates allows a determination of the magnitude of shear-tension coupling that can be obtained with varying magnitudes of anisotropy, as well as the impact on the various components of strength and modulus. Laminates 10, 11 and 12 reflect variations on Laminate 7 in which the off-axis fibers are oriented at angles of 10°, 15°, and 25°. By comparing the results for laminates 7, 10, 11 and 12, it should be possible to discern the influence of fiber angle on the shear-tension coupling, strength and modulus. Laminates 13 through 16 are designed to investigate alternative skin arrangements in which the $\pm 45^\circ$ glass fibers are either oriented differently ($+20^\circ/-70^\circ$) or are replaced by entirely different glass skin reinforcement fibers ($+75^\circ/-55^\circ$, -70° or 90°). Finally, laminate 21 is designed to reflect a biaxial ($\pm 45^\circ$) carbon fiber complex.

Tensile strength and modulus tests were performed on all laminates in the 0° material orientation. In the 90° material orientation, tensile tests were performed on laminate items 1 through 16. Compressive strength and modulus tests were performed on laminate items 1 through 16. In-plane shear strength and modulus tests were performed on all laminates. Interlaminar shear strength tests were performed on items 1 through 16. Edgewise compression tests were performed on laminates items 5 through 16. Details of the testing are presented in Section 3.

Analysis of the laminates was performed using classical lamination theory (CLT) and finite element analysis (FEA). Classical lamination theory was utilized to characterize the influence of the end constraints on the elastic properties of the anisotropic laminates. CLT was also used to determine the level of coupling in the anisotropic laminates. Finite element analysis was utilized to perform a linear first ply failure analysis of the laminates in tension and compression. Details of the analysis are presented in Section 4.

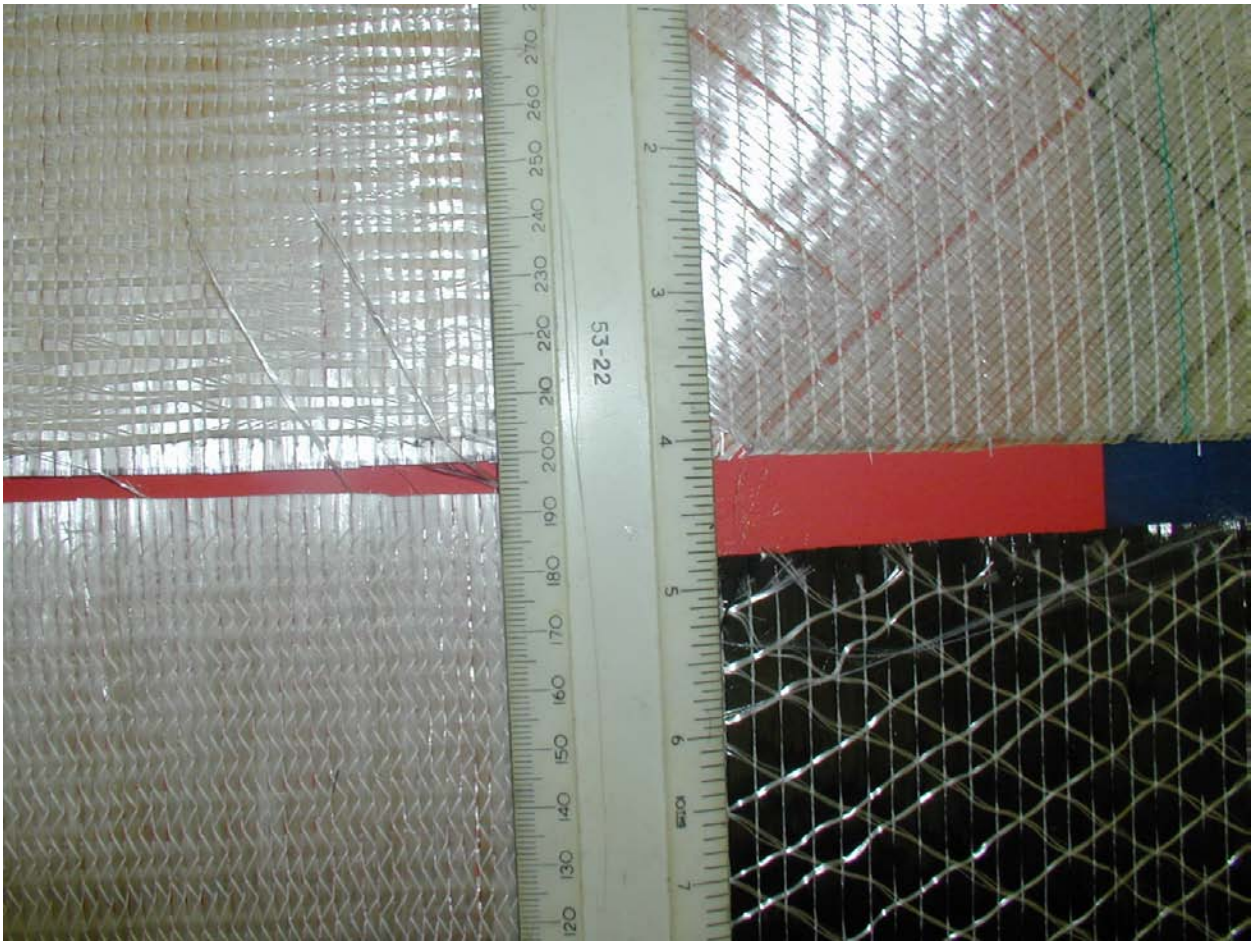

Figure 1.1: Constitutive fiber complexes. (Clockwise from upper right: 12 oz/yd^2 double bias glass, 15 oz/yd^2 unidirectional carbon, 6 oz/yd^2 unidirectional glass, 16 oz/yd^2 unidirectional glass.)

Table 1.1: Constitutive fiber complexes.

Saertex style number: S32CU970-00520-1270-264000
15 oz/yd^2 Unidirectional Carbon Fabric

- 0° carbon fibers (24,000 tows) of nominal areal weight 502 g/m^2 (14.81 oz/yd^2)
- 90° Polyethersulfone(PES) fibers of nominal areal weight 4 g/m^2
- +60° E-glass fibers of nominal areal weight 6 g/m^2
- −60° E-glass fibers of nominal areal weight 6 g/m^2

The four layers are stitch bonded with nominal 6 g/m^2 PES fibers.

Saertex style number: S35EU990-00210-1270-464018
6 oz/yd^2 Unidirectional Glass Fabric

- 0° E-glass fibers of nominal areal weight 213 g/m^2 (6.28 oz/yd^2)
- Random mat E-glass fibers of nominal areal weight 35 g/m^2 (0.94 oz/yd^2)

The two layers are stitch bonded with nominal 12 g/m^2 PES fibers.

Saertex style number: S15EU910-00580-1200-100000
16 oz/yd^2 Unidirectional Glass Fabric

- 0° E-glass fibers(1,200 tows) of nominal areal weight 528 g/m^2 (15.57 oz/yd^2)
- 90° E-glass fibers(68 tows) of nominal areal weight 54 g/m^2 (1.59 oz/yd^2)

The two layers are stitch bonded with nominal 18 g/m^2 PES fibers.

Saertex style number: U32EX010-00400-1270-264000
12 oz/yd^2 Double Bias (±45°) Glass Fabric

- +45° E-glass fibers of nominal areal weight 200 g/m^2 (5.90 oz/yd^2)
- −45° E-glass fibers of nominal areal weight 200 g/m^2 (5.90 oz/yd^2)

The two layers are stitch bonded with nominal 6 g/m^2 PES fibers.

Saertex style number: U32EX010-01291-1270-264000
38 oz/yd^2 Double Bias (±45°) Glass Fabric

- +45° E-glass fibers of nominal areal weight 643 g/m^2 (18.96 oz/yd^2)
- −45° E-glass fibers of nominal areal weight 643 g/m^2 (18.96 oz/yd^2)

The two layers are stitch bonded with nominal 6 g/m^2 PES fibers.

Table 1.2: Composite laminates.

Laminate	Style	Schedule	Layers	Behavior	Note
1	SC/GUD	$[(0_G)_8]$	8	Orthotropic	
2	SC/CUD	$[(0_C)_6]$	6	Orthotropic	
3	85GUD/15GDB	$[\pm 45_G/(0_G)_4]_s$	10	Orthotropic	
4	85CUD/15GDB	$[\pm 45_G/(0_C)_3]_s$	8	Orthortopic	
5	55CUD/30C20/15GDB	$[\pm 45_G/20_C/(0_C)_2]_s$	8	Coupled, Extension/Shear	
6	55GUD/30C20/15GDB	$[\pm 45_G/0_G/20_C/0_G/\overline{0}_G]_s$	9	Coupled, Extension/Shear	
7	30CUD/55C20/15GDB	$[\pm 45_G/(20_C)_2/0_C]_s$	8	Coupled, Extension/Shear	
8	15CUD/70C20/15GDB	$[\pm 45_G/(20_C)_2/0_C/(20_C)_3/\mp 45_G]$	8	Coupled, Extension/Shear/Bend	
9	10GUD/75C20/15GDB	$[\pm 45_G/(20_C)_2/0_G/(20_C)_3/\mp 45_G]$	8	Coupled, Extension/Shear/Bend	
10	30CUD/55C10/15GDB	$[\pm 45_G/(10_C)_2/0_C]_s$	8	Coupled, Extension/Shear	
11	30CUD/55C15/15GDB	$[\pm 45_G/(15_C)_2/0_C]_s$	8	Coupled, Extension/Shear	
12	30CUD/55C25/15GDB	$[\pm 45_G/(25_C)_2/0_C]_s$	8	Coupled, Extension/Shear	
13	30CUD/55C20/15G75-55	$[75_G/-55_G/(20_C)_2/0_C]_s$	10	Coupled, Extension/Shear	1
14	85CUD/15G20-70	$[(+20/-70)_G/(0_C)_3]_s$	8	Coupled, Extension/Shear	2
15	30CUD/55C20/15G-70	$[(-70_G)_2/(20_C)_2/0_C]_s$	10	Coupled, Extension/Shear	1
16	30CUD/55C20/15G90	$[(90_G)_2/(20_C)_2/0_C]_s$	10	Coupled, Extension/Shear	1
18	SK/GDB	$[(\pm 45_G)_6]_s$	12	Quasi-Isotropic	
20	SK/GDB	$[(\pm 45_G)_2]_s$	4	Quasi-Isotropic	3
21	SK/CDB	$[(+45_C/-45_C)_2]_s$	8	Quasi-Isotropic	

Notes	
1	6 oz/yd^2 unidirectional glass
2	± 45 double bias glass rotated 20°
3	38 oz/yd^2 ± 45 double bias glass

Style abbreviations are: SC-Sparcap; SK-Skin; CUD-Carbon Unidirectional; GUD-Glass Unidirectional; GDB-Glass Double Bias. Numbers in the style indicate percent by volume: 85GUD/15GDB is 85% unidirectional glass, 15% double bias glass by volume. Schedule definitions are per ASTM Standard D6507-00(2005): Standard Practice for Fiber Reinforcement Orientation Codes for Composite Materials; with subscripts added to denote the material: C-Carbon; G-Glass. $\pm 45_G$ indicates $12 oz/yd^2$ double bias glass unless noted otherwise.

2. Laminate Fabrication using VARTM

The laminates evaluated in this study were fabricated using a vacuum assisted resin transfer molding (VARTM) process. The VARTM process is a derivative of resin transfer molding (RTM). It differs from RTM primarily by eliminating the need for matched-metal tooling and resin injection equipment. With VARTM, the pre-form is stacked on a metal tool and a conformal vacuum bag replaces the matched metal tool. Instead of injecting the resin under pressure, the bagged pre-form is placed under a vacuum which draws resin through a port from a reservoir.

The first step in the VARTM process is stacking the pre-form on the metal tool. Inlet and outlet ports are positioned around the pre-form as required. The pre-form and ports are sealed under a conformal bag. Respective ports from the bagged pre-form are attached to the resin reservoir and the vacuum pump. When a vacuum is established in the bagged pre-form, the resin inlet ports are opened to infuse the pre-form. Infusion is complete when resin is observed in the outlet ports. When the infusion is complete, the ports are closed, maintaining the vacuum, and the part is cured. Details of the VARTM process used in this study are described in this section. A picture of the VARTM setup and a panel being infused is presented in Figure 2.1.

(a) VARTM Equipment

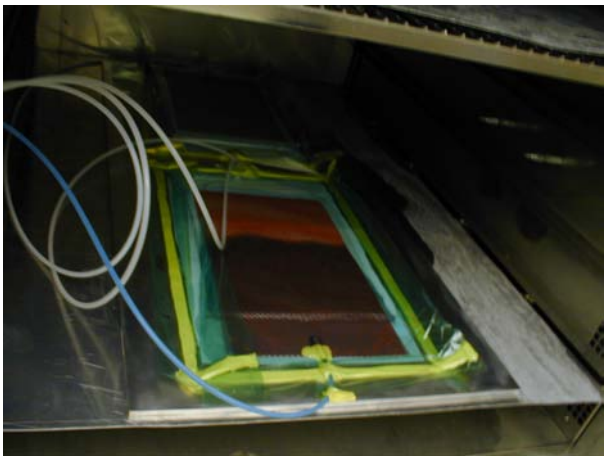

(b) Panel Infusion

Figure 2.1: VARTM panel infusion and equipment.

2.1 Aluminum Tool

Three flat aluminum tools measuring 116.8-cm long by 53.3-cm wide by 8.5-mm thick were constructed for this study. The tool surface was ground with a hand held flat grinder until all visible blemishes were removed from the surface. Then the tools were tested for flatness using a coordinate measuring machine(CMM). Approximately 200 points were measured by probe for each tool. The measurements were analyzed to evaluate flatness utilizing the Geomeasure software. A flatness of 0.762-mm was maintained on all tools. Small holes in the tools were sealed using B-15 mold sealer.

The tools were coated with six layers of Frekote NC 44 releasing agent. Each coat was applied in intervals of 15 minutes. The tools were then cured in the oven for 30 minutes at 215° F. After every 6-8 uses, one layer of Frekote NC 44 was applied to maintain the de-molding property.

2.2 Bagged Pre-Form

A Masonite template measuring 91.4-cm long by 45.7-cm wide by 0.635-cm thick was utilized to cut the fabrics for stacking. For the 10°, 15°, 20° and 25° oriented layers, three right triangles with a hypotenuse measuring 91.4-cm long were utilized to orient the Masonite template. After being cut, the fabric was stacked and aligned to boundaries drawn on the tool. After all of the layers were stacked on the tool, quarter inch polyethylene tubing was positioned at each end to provide injection and vacuum ports. Next, two layers of flow media were stacked on the fabric. The flow media measured 96.5-cm long by 45.7-cm wide. It was offset 7.62-cm towards the injection port leaving 2.54-cm of composite fabric without flow media near the vacuum port. Finally, the entire assembly was sealed under a vacuum bag. The components utilized to bag the pre-form are listed in Table 2.1. A sketch of the bagged pre-form is presented in Figure 2.2. After bagging the pre-form, the vacuum integrity of the seal was verified. A vacuum loss of less than 1-in Hg per 12 hours was defined as the acceptable limit.

Table 2.1: Components of the VARTM bagging.

Component	Product Identification
Flow media	Delstar #141-4336
Peel-ply	Decomp D4444
Sealant	Airtech AT-200Y
Vacuum bag	Decomp D316

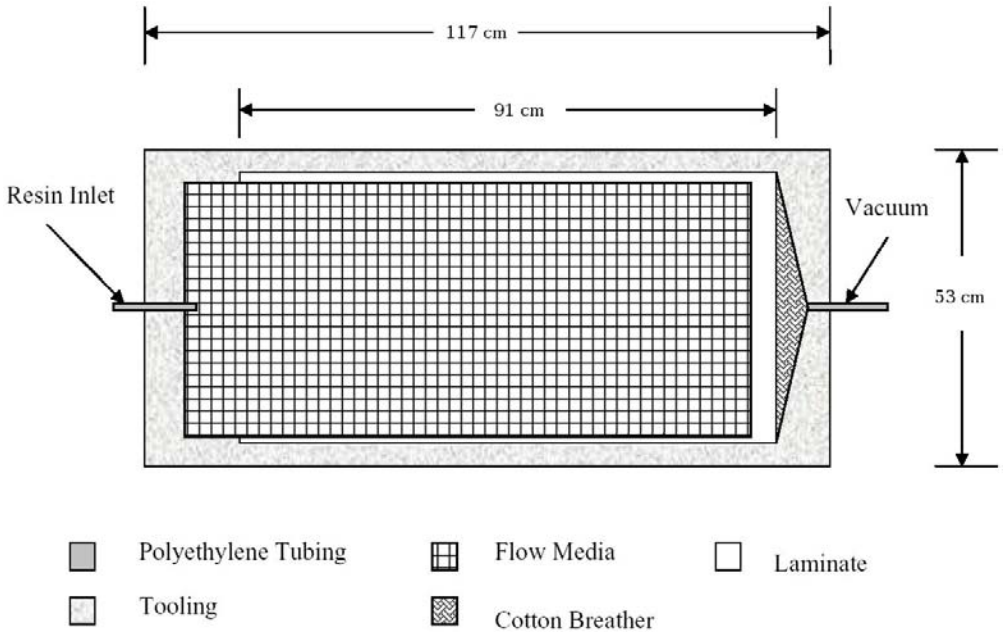

Figure 2.2: The bagged pre-form.

2.3 Infusion, Curing & Post-Curing

The bagged pre-form was checked for vacuum integrity and left over night, after which the vacuum integrity of the bagged pre-form was checked. After ensuring that the vacuum loss in the bagged

part was less than 1 in-Hg, it was placed in the oven and the heating cycle program was switched on. Through the side opening of the oven, all the tubes from the bagged part were pulled out and labeled as inlet or outlet, depending upon the location of the port. The outlet port was connected to the resin trap and the inlet port was left to be dipped in the conditioned resin system. While the oven was ramping up to $30°C$, resin and hardener were poured in separate paper cups. Both the resin and hardener were then placed in the oven along side the bagged pre-form. After conditioning the resin system to a temperature of $30°C$, the resin and hardener were removed from the oven. Resin and hardener were then mixed in the ratio of 100:30 by weight. A wooden tongue depressor was used to stir the mix properly. In the meantime, the oven temperature ramped up to $35°C$ and maintained at that temperature for another two hours.

While the resin was being conditioned in the oven, the vacuum pump was switched on and the vacuum integrity of the system without the bagged part was checked. Once the part was conditioned at $35°C$, and the system connected, the outlet valve of the part connected to the resin trap was opened. The inlet port tube was then dipped into the paper cup containing the conditioned resin system. The inlet valve was then opened to begin infusion. Once the resin exits the outlet port and enters the resin trap, both the inlet and outlet valves were closed and the vacuum pump turned off. A sketch of the VARTM system is presented in Figure 2.3.

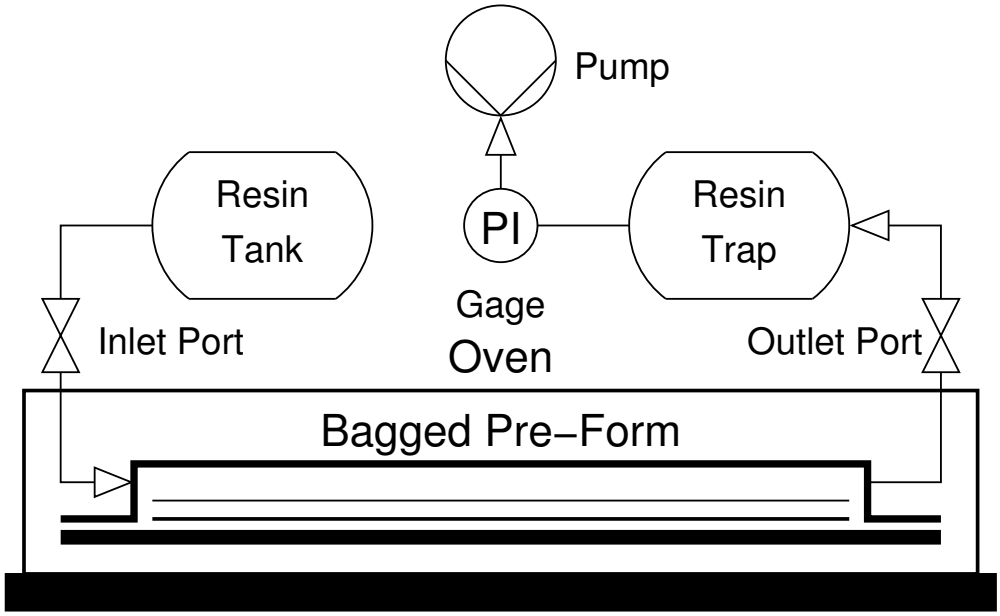

Figure 2.3: Vacuum assisted resin transfer molding.

The procedure to infuse, cure and post-cure the laminates is summarized by:

1. Check the vacuum integrity of the bagged part one day prior to infusion and leave it over night.
2. Ensure that the loss in vacuum is less than 1 in-Hg in the same part, next morning.
3. Place the part in the oven and connect the outlet tube to the resin trap.
4. Turn on the oven and let the temperature climb up to 30 deg. C in 15 minutes.
5. During these 15 minutes, pour resin and hardener in two separate paper cups and place them along side the tool in the oven.

6. The oven temperature remains at 30 deg. C for 40 minutes in order to condition the resin and hardener.

7. Resin and hardener are removed from the oven at the end of this cycle and mixed together in the ratio 100:30 by weight.

8. The oven temperature ramps up to 35 deg. C in the meantime and holds at this stage for 2 hours.

9. Pre-heat the tooling in the oven at $35°C$ for one hour.

10. Start the vacuum pump.

11. When a vacuum of 28 in-Hg is achieved, connect the closed vacuum and injection port valves to the respective ports routed from the oven.

12. Open the vacuum port valve and verify the bag vacuum integrity.

13. Open the injection port valve to initiate the resin infusion.

14. Close the vacuum port valve when resin starts entering the resin trap.

15. Turn off the vacuum pump.

16. Ramp the oven temperature to $60°C$ in one hour and hold for six hours.

17. Ramp up the oven temperature to $85°C$ in one hour and hold for two hours.

18. Ramp up the oven temperature to $100°C$ over in one hour and hold for two hours.

19. Ramp down the oven temperature to ambient in one hour.

20. Cut all the tubes using a knife and pull the part with tool out of the oven.

21. De-mold the laminate from the tool.

The post-cure was designed to simulate the effects of storage of the material for 6 months at ambient conditions. Note that all fabrication was performed without humidity control.

The time required to infuse the laminate was determined by the permeability of the fabric. Fabrics with lower permeability required more time to infuse. The permeability of a fabric is related to the diameter, fabric construction, tow separation, fiber orientation with respect to the resin flow direction, viscosity of the resin, packing density of the fibers and the filament diameter. Fabrics with large diameters exhibit lower permeability. The filament diameter of the carbon used in this study was 7 μm and the glass was greater than 15 μm. Therefore, laminates comprised mostly of carbon infused faster than laminates comprised mostly of glass. The variation of infusion times with laminate is listed in Table 2.2.

Physical testing was performed on the laminates to evaluate the VARTM process. The laminates were evaluated based on fiber volume fraction, V_f, using ASTM D2584,[1] void content, ϕ_a, using ASTM D2734,[2] and density, ρ, using ASTM D792,[3] the results of which are listed in Table 2.2. A complete presentation of the physical test results is presented in Appendix A. The method employed to measure the fiber volume fraction for hybrid composites deviated from the standard practice. The burn off temperature as per the standard is supposed to remain at $565 \pm 30°C$, or other temperature compatible with the composite system, that will burn off the matrix and leave

Table 2.2: VARTM infusion times and physical test results.

Laminate	Infusion Time (min)	Fiber Volume Fraction - V_f (%)	Void Fraction ϕ_a (%)	Density ρ (kg/m^3)
1	45	48.3	-0.74	1,855
2	27	60.2	-1.09	1,550
3	38	48.6	-0.36	1,855
4	27	54.9	-1.29	1,605
5	34	54.2	-1.19	1,605
6	32	48.3	-1.40	1,772
7	24	52.3	-1.20	1,578
8	27	53.6	-1.23	1,578
9	24	46.3	0.34	1,550
10	27	53.2	-2.06	1,605
11	27	52.5	-1.17	1,578
12	23	54.4	-0.44	1,578
13	26	43.4	-0.17	1,495
14	24	53.9	-1.68	1,605
15	23	44.7	-1.32	1,522
16	27	43.0	-1.25	1,522
18	19	47.5	0.39	1,827
20	25	55.0	-0.19	1,938
21	18	56.1	-1.84	1,550

the reinforcement. In order to ensure that carbon reinforcement does not burn off, a temperature of $500°C$ was used for all hybrid composites. The void content was dependent on the resin system, fiber geometry and external leaks. In addition to the fabrication process, fiber volume fraction was affected by separation of the fiber tows and gaps due to stitch bonding, which reduced the fiber volume fraction. Properties of the laminates presented in the succeeding sections were not corrected for fiber volume fraction because the variation between laminates appeared to be dependent on the fabric and matrix rather than the fabrication process.

The values for void content shown in Table 2.2 are generally negative. Calculation of the void content uses the values for the fiber volume fraction measured previously. Given uncertainties in this measurement as well as uncertainties in the processes employed in measuring void content, it is not uncommon to obtain small negative values for coupons that have very low void content. In the present testing, however, calculation of void fraction was further complicated by the hybrid nature of most of the laminates, where assumptions had to be made about the ratio of glass to carbon in each coupon based upon the nominal areal weights of the constitutive materials. However, the areal weight varies from the nominal weight and varies from region to region of each fabric, and all of these factors introduce uncertainty in to the calculation. Since the results are small negative numbers, however, we believe this suggests that our void content was generally quite small.

3. Laminate Testing

Mechanical testing was performed to measure the elastic properties and strength of the laminates. Elastic properties and strength were determined from tensile, compressive and in-plane shear testing. Interlaminar shear strength tests were performed. Out-of-plane displacement, axial strain, transverse strain and in-plane shear strain measurements were taken using photogrammetry data from edgewise compression tests. All testing was performed at ambient temperature and humidity. Details of the testing are presented in this section.

3.1 Tensile Testing

Tensile specimens were tested per ASTM Standard D3039-00.[4] The specimens were nominally 22.86-cm long by 2.56-cm wide with thicknesses varying with laminate schedule. Tabs were required on the tension specimens and measured 5.08-cm long and 0.157-cm thick. This resulted in a nominal gauge section of 12.7-cm. A sketch of the specimen is presented in Figure 3.1.

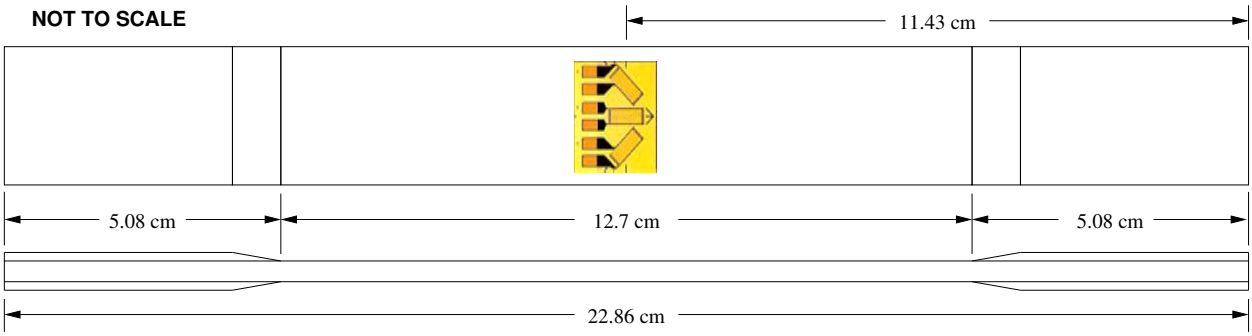

Figure 3.1: Tensile test specimen.

Initially, a 10.16-cm wide untabbed specimen was utilized but failure occurred in the grips of the test fixture. A 2.08-cm wide untabbed specimen was tested but also failed in the grips. Coupons machined with a dog-bone gauge section were judged unacceptable due to broken fibers, especially at the free edges. Acceptable failures were obtained with the ASTM D3039 tabbed tension specimen.

Tension tests were performed in the axial, or 0° material orientation, and the transverse, or 90° material orientation. The strains were measured using either biaxial gauges or rectangular rosettes, shown in Figure 3.2.

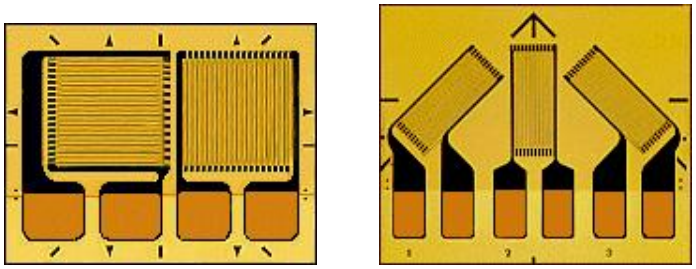

(a) Biaxial Rosette (b) Rectangular Rosette

Figure 3.2: Strain gauges used in the tensile tests.

The test frames were calibrated and aligned per ASTM-E4 which specifies that the load reading should be within 1% of the target value. Testing was performed on an MTS Alliance RF/300 electromechanical load frame with a 300-KN load cell and on an MTS 810 Materials System load frame with a 245-KN load cell. The Alliance test fixture is presented in Figure 3.3. For each test, the load, crosshead deflection and strain at the center of the gauge section was measured. Loading was applied at 0.127 cm/min. A summary of the tensile testing is listed in Table 3.1.

Table 3.1: Laminates tested for tensile strength & modulus.

	0°		90°	
Laminate	Number	Gauge	Number	Gauge
1	3	Biaxial gauge	3	Biaxial gauge
2	3	Biaxial gauge	3	Biaxial gauge
3	3	3–gauge rosette	3	Biaxial gauge
4	3	3–gauge rosette	3	Biaxial gauge
5	3	3–gauge rosette	3	3–gauge rosette
6	3	3–gauge rosette	3	3–gauge rosette
7	3	3–gauge rosette	3	Biaxial gauge
8	3	3–gauge rosette	3	Biaxial gauge
9	3	3–gauge rosette	3	Biaxial gauge
10	3	3–gauge rosette	3	Biaxial gauge
11	3	3–gauge rosette	3	3–gauge rosette
12	3	3–gauge rosette	3	3–gauge rosette
13	3	3–gauge rosette	3	Biaxial gauge
14	3	3–gauge rosette	3	Biaxial gauge
15	3	3–gauge rosette	3	Biaxial gauge
16	3	3–gauge rosette	3	Biaxial gauge
18	3	Biaxial gauge		
20	3	Biaxial gauge		
21	3	Biaxial gauge		

Figure 3.3: Tensile test fixture.

3.2 Compressive Testing

Compressive specimens were tested for failure and modulus per SACMA Recommended Method SRM-1.[5] The specimens were nominally 8.08-cm long by 1.27-cm wide. Separate tests were performed for the failure and modulus. Failure specimens were tabbed over 3.81-cm at each end, resulting in a gauge length of 0.478-cm, Figure 3.5a. This, combined with the anti-buckling fixture presented in Figure 3.4, was required to obtain compressive failure. As a consequence of the compressive failure specimen gauge length, it was not possible to instrument the specimen with a strain gauge. Compressive modulus test specimens were identical to the failure specimens without the tabs, Figure 3.5b. This allowed the specimen to be instrumented with a uniaxial strain gauge.

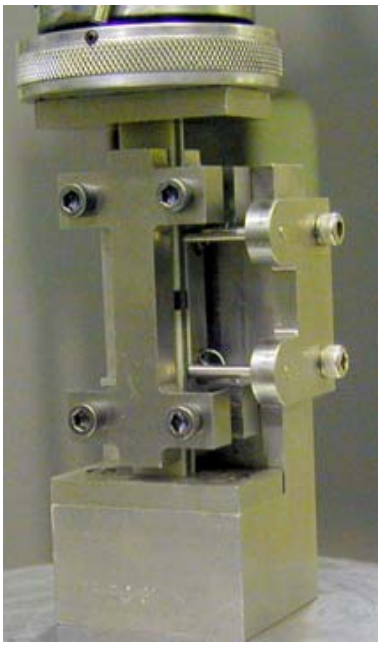

Figure 3.4: Compressive strength test fixture.

Three modulus and three failure specimens were tested for each laminate. All compression tests were performed in the axial direction of the laminate. The test frames were calibrated and aligned per ASTM-E4 which specifies that the load reading should be within 1% of the target value. Compressive testing was performed on an MTS 810 Materials System load frame with a 98-KN load cell. For each test, the load and crosshead deflection were measured. Loading was applied at 0.127 cm/min. For the modulus tests, strain measurements with uniaxial gauges were taken at the gauge center. Three modulus and three failure specimens were test for each laminate except laminate 16 (the 12 oz/yd^2 double bias glass material). Successful tests of laminate 16 were not obtained due to problems with specimen buckling.

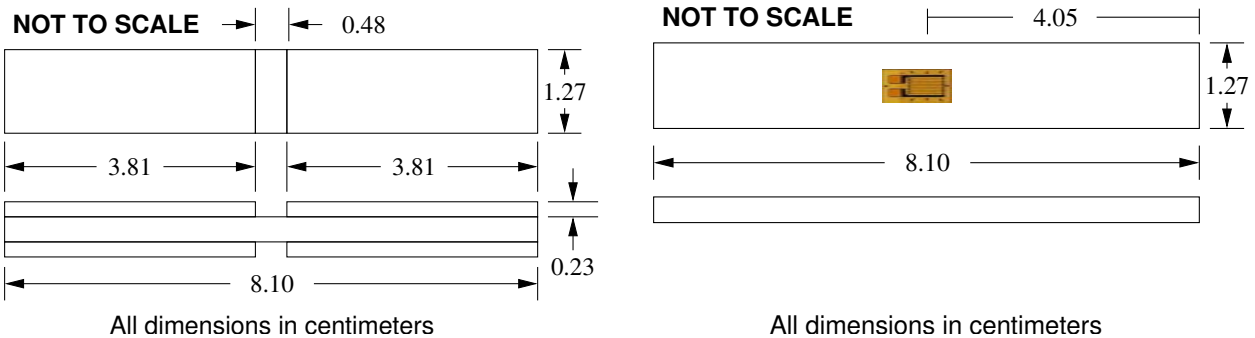

(a) Strength (b) Modulus

Figure 3.5: Compressive test specimens.

3.3 In-Plane Shear Testing

In-plane shear specimens were tested for failure and modulus per ASTM Standard D5379-98[6] (Figure 3.6). The V-notched specimens were nominally 7.62-cm long by 1.91-cm wide with a 1.14-cm wide notch that was machined into the specimen. A notch angle of 90° was machined into all specimens.

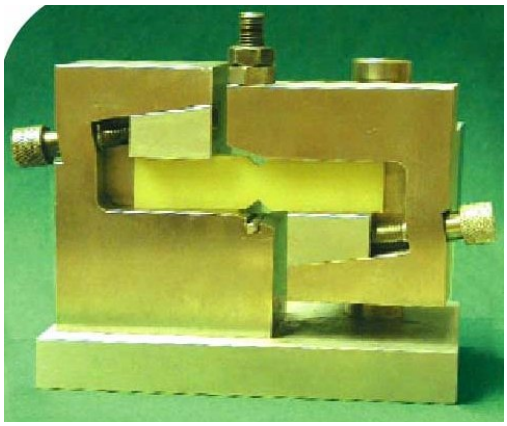

Figure 3.6: In-Plane shear test fixture.

Three specimens were tested for each laminate. The test frames were calibrated and aligned per ASTM-E4 which specifies that the load reading should be within 1% of the target value. The specimens were instrumented with 2 strain gauges oriented at ±45 degrees, Figure 3.7. For each test, the load, crosshead deflection and strain at the center of the gauge section was measured. In-plane shear testing was performed on an MTS 810 Materials System load frame with a 98-KN load cell. For each test, the load and crosshead deflection were measured. Loading was applied at 0.127 cm/min.

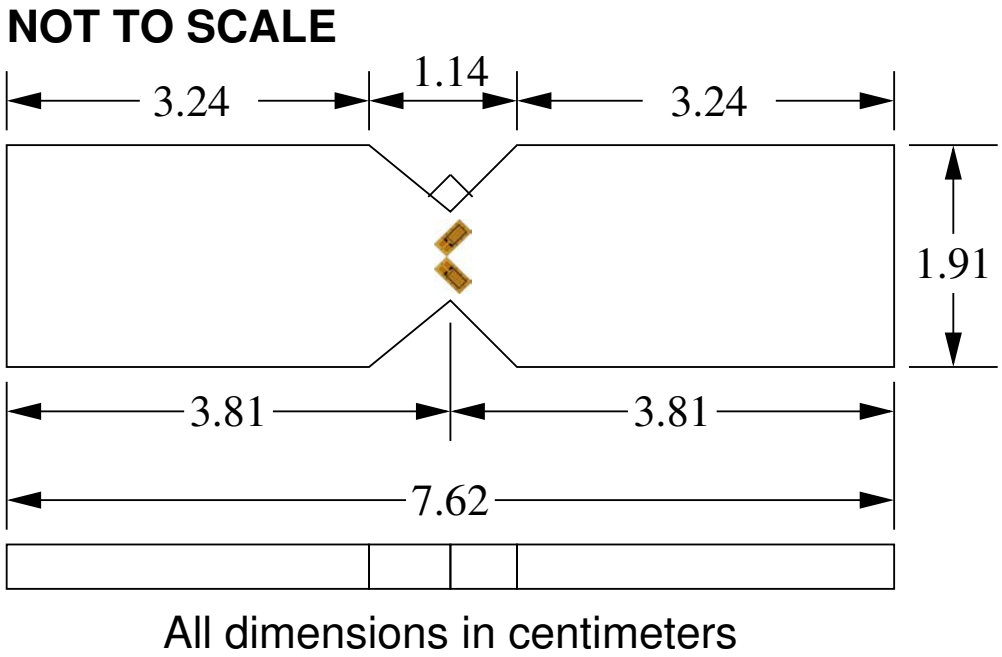

Figure 3.7: In-Plane shear test specimen.

3.4 Interlaminar Shear Strength

Interlaminar shear specimens were tested for failure per ASTM Standard D2344[7] (Figure 3.8). Three specimens were tested for each of laminates 1 through 16. Development testing of interlaminar shear specimens was performed to ensure interlaminar failures were obtained and not tensile or compressive failure.

Three specimens were tested for each laminate. The test frames were calibrated and aligned per ASTM-E4 which specifies that the load reading should be within 1% of the target value. For each test, the load and crosshead deflection were measured.

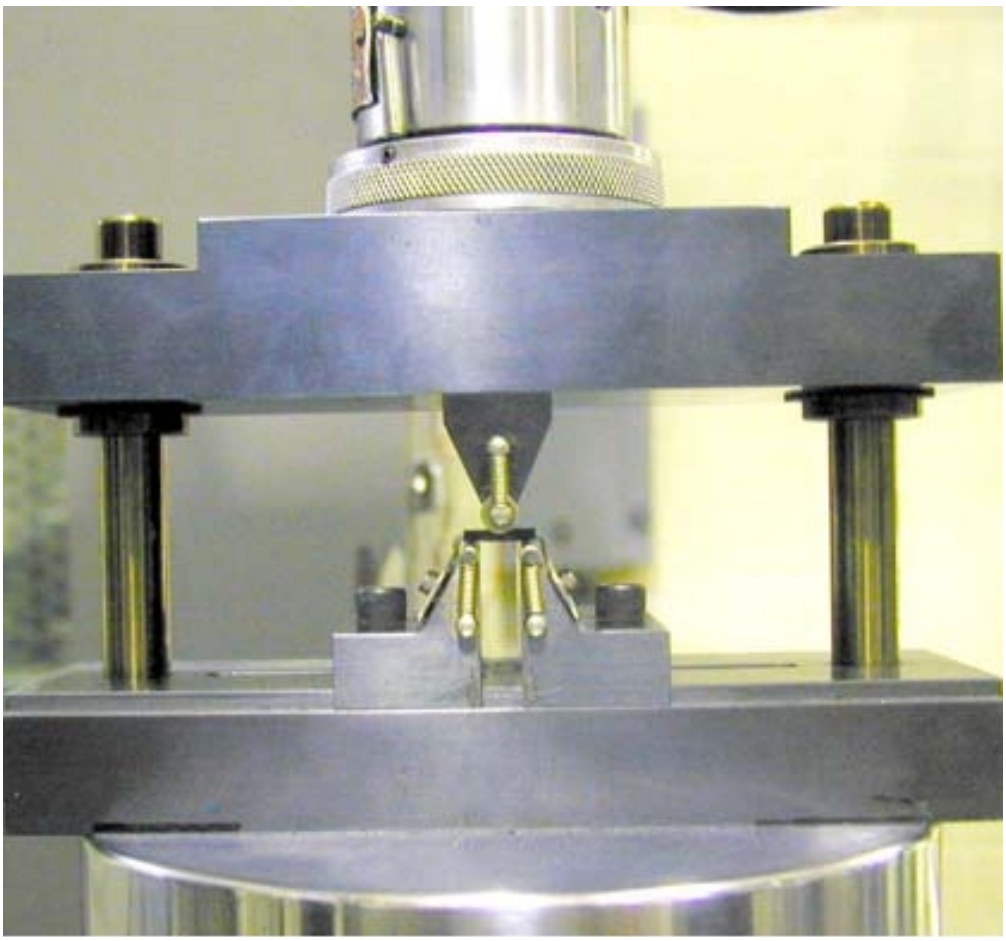

Figure 3.8: Interlaminar shear test fixture.

3.5 Edgewise Compression

Edgewise compression testing was performed on laminates 5 through 16. The test specimens were rectangular panels measuring 22.86-cm long by 11.43-cm wide. The test frames were calibrated and aligned per ASTM-E4 which specifies that the load reading should be within 1% of the target value. Out-of-plane displacement, axial strain, transverse strain and in-plane shear strain measurements were taken using the ARAMIS photogrammetry data acquisition system.[8] A camera resolution of $1280x1024$ pixels was utilized that enabled resolution of strains from 0.02% to 100%.

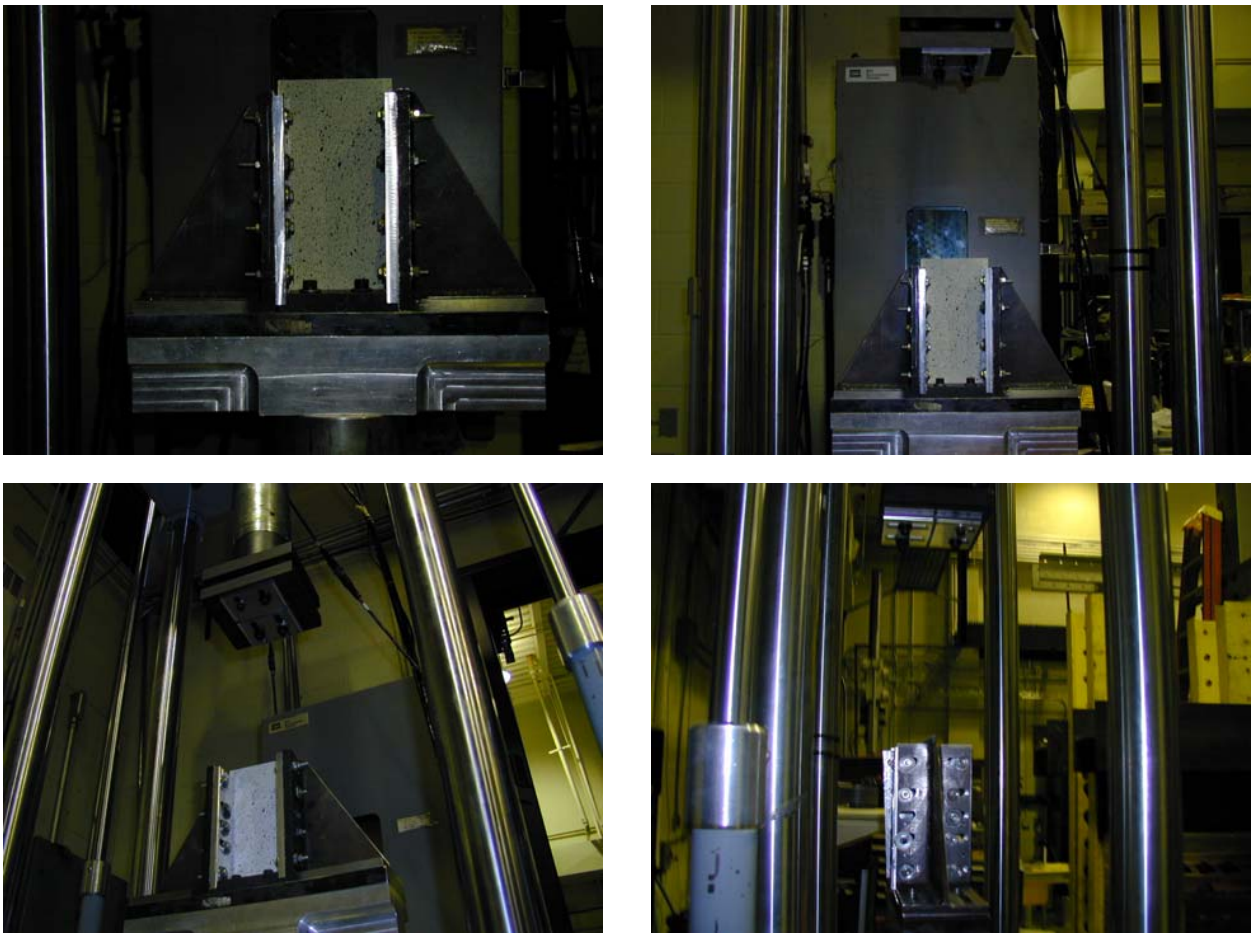

Figure 3.9: Edgewise compression test fixture.

4. Laminate Test Results & Analysis

The test data was reduced to characterize the elastic properties and strength of the laminates. A classical lamination theory analysis of the anisotropic laminates was performed to characterize the effect of end constraints on the moduli. The CLT analysis was also used to characterize the level of extension/shear coupling in the anisotropic laminates. Appropriate use of the material properties was examined with a first ply failure finite element analysis of each laminate. Details of the test results and analysis are presented in this section.

4.1 Laminate Test Results

The data measured from the mechanical testing described in Section 3 was used to calculate the elastic properties and strength of the laminates. Tensile modulus, tensile strength and Poisson's ratio were calculated from the tensile test data. Compressive modulus and strength was calculated from the compressive test data. In-plane shear modulus and strength was calculated from the in-plane shear test data.

Corrections were required of the strain data measured with the biaxial strain gauges and rectangular rosettes. Transverse sensitivity corrections were performed based on Micro Measurements Technical Note 509.[9] Further processing was required of the strain measured with the rectangular rosettes, all of which were oriented 45° to the material axes. To obtain the strain oriented with the material axes, the full strain tensor measured with the rectangular rosettes was rotated 45°.

The elastic properties were calculated according to the respective standard. Remote load and strain in the gauge section were directly measured in the tests. Remote stress was calculated from the remote load and the initial cross-sectional area in the gauge of the test specimen. For tensile and compressive elastic properties, the standards recommend using the range $1,000$ to $3,000$ $\mu strain$, which was used to reduce this data. For the in-plane shear modulus, the standard recommends using a $4,000$ $\mu strain$ range with the lower limit in the range of $1,500$ to $2,500$ $\mu strain$. In-plane shear modulus was determine using the range $2,500$ to $5,500$ $\mu strain$. A summary of the test results is listed in Table 4.1. The complete presentation of the test data is presented in Appendix A, contained in Volume 2.

In general, the standards apply to balanced and symmetric laminates. Using these methods to process the data measured from the anisotropic laminates can result in an error that is attributed to end constraints.[10–13] The influence of end constraints on the elastic properties of the anisotropic laminates is addressed later in this section. Data presented in Table 4.1 has not been corrected for end constraints.

Material strength of the laminates was determined from visual inspection of the load versus strain. For laminates that exhibit linear elastic response to failure, the strength is unambiguous. For laminates that exhibit nonlinear or plastic behavior, the point of failure is not well defined. For these laminates, failure was defined as the load at which a rapid increase in the strain was observed; this load was generally slightly less than the maximum load at which complete failure of the coupon occurred or at which the test was terminated. Nonlinear behavior was most pronounced in the shear data. The ASTM standards for shear testing prescribe that ultimate shear strain is the minimum of the value at failure or 5% strain. As noted in the testing section, strain measurements were not available from the compressive strength testing. An estimate of the compressive strain allowable was obtained from the compressive strength and modulus recognizing that the unidirectional laminates exhibited linear elastic behavior to failure in compression.

Table 4.1: Strength and modulus summary data.

		Tension 0°			Tension 90°			Compression		In-Plane Shear		Interlaminar
Laminate	Style	E_x (GPa)	ν_{xy} (—)	X_t (MPa)	E_y (GPa)	ν_{yx} (—)	Y_t (MPa)	E_x^c (GPa)	X_c (MPa)	G_{xy} (GPa)	S (MPa)	Shear (MPa)
1	SC/GUD	36.5	0.257	703.9	12.6	0.093	58.3	37.9	791.1	3.9	62.5	56.1
2	SC/CUD	127.3	0.328	1585.3	8.8	0.023	34.2	122.8	956.2	5.1	73.6	67.5
3	85GUD/15GDB	32.9	0.310	673.5	13.3	0.128	107.1	33.9	684.9	5.7	108.3	52.3
4	85CUD/15GDB	108.5	0.345	1288.0	10.7	0.037	57.1	97.5	985.9	6.5	119.8	57.1
5	55CUD/30C20/15GDB	85.7	0.587	1212.1	11.0	0.045	52.1	86.5	827.1	8.6	120.8	56.5
6	55GUD/30C20/15GDB	38.9	0.413	589.3	12.0	0.120	99.9	39.9	551.0	7.0	126.2	54.2
7	30CUD/55C20/15GDB	65.2	0.611	710.2	10.5	0.089	56.0	62.7	543.8	9.3	130.2	50.4
8	15CUD/70C20/15GDB	50.5	0.595	463.6	10.1	0.133	54.0	49.9	396.7	9.0	145.3	54.0
9	10GUD/75C20/15GDB	29.2	0.591	269.4	9.3	0.170	54.5	31.3	329.8	6.5	116.2	51.5
10	30CUD/55C10/15GDB	88.9	0.520	826.5	10.0	0.066	102.7	96.3	771.9	6.7	125.8	54.2
11	30CUD/55C15/15GDB	70.2	0.574	795.3	8.0	0.144	55.5	69.3	614.3	7.5	130.3	53.0
12	30CUD/55C25/15GDB	55.7	0.589	667.9	10.9	0.084	56.8	54.6	521.4	11.0	135.7	46.1
13	30CUD/55C20/15G75-55	48.8	0.509	466.1	11.1	0.106	55.0	50.6	413.6	7.7	123.9	40.8
14	85CUD/15G20-70	107.7	0.267	1298.5	10.1	0.036	57.4	97.0	937.4	5.2	96.0	59.6
15	30CUD/55C20/15G-70	50.0	0.493	525.2	11.5	0.138	62.6	51.1	386.0	6.6	119.1	40.1
16	30CUD/55C20/15G90	52.1	0.292	490.0	12.3	0.083	63.4	52.1	409.8	6.3	99.2	39.4
18	SK/GDB12	11.1	0.556	112.4	11.1	0.653	119.1	—	—	10.1	122.6	38.6
20	SK/GDB38	12.3	0.634	104.8	12.3	0.574	95.1	14.9	168.2	13.4	128.0	24.5
21	SK/CDB	13.8	0.726	118.4	—	—	—	16.2	180.9	17.9	137.5	28.7

Refer to Table 1.2 for style definitions.

4.2 Constitutive Lamina Properties

Laminates 1, 2, 18 and 20 were utilized to calculate the constitutive properties of the unidirectional glass/epoxy, unidirectional carbon/epoxy and two types of double bias glass/epoxy lamina, listed in Table 4.2.

Table 4.2: Constitutive lamina properties.

Property	Units	Unidirectional Glass/Epoxy $16oz/yd^2$	Unidirectional Carbon/Epoxy $15oz/yd^2$	Double Bias Glass/Epoxy $12oz/yd^2$	Double Bias Glass/Epoxy $38oz/yd^2$
E_x	GPa	36.5	127.3	11.1	12.3
E_y	GPa	12.6	8.78	11.1	12.3
ν_{xy}	—	0.257	0.328	0.604	0.604
G_{xy}	GPa	3.94	5.07	10.1	13.4
X_t	MPa	703.9	1,585	112.4	104.8
Y_t	MPa	58.3	34.2	119.1	95.1
S	MPa	62.5	73.6	122.6	128.1
X_c	MPa	791.1	956.2	—	168.2
ϵ_{xt}	strain	2.00%	1.20%	4.99%	4.99%
ϵ_{yt}	strain	1.01%	0.39%	4.99%	4.99%
γ_{xy}	strain	5.00%	5.00%	1.22%	0.97%
ϵ_{xc}	strain	2.09%	0.78%	—	1.13%
V_f	%	48.3	60.2	47.5	55.0
ρ_f	kg/m^3	2,600	1,800	2,600	2,600

4.2.1 $16oz/yd^2$ Unidirectional Glass/Epoxy Laminate Behavior

Test results for the unidirectional glass/epoxy laminate are presented in Figures 4.1 through 4.4. It exhibited linear-elastic behavior to failure in tension (Figure 4.1) and compression in the axial direction (Figure 4.3). In the transverse direction, the tension behavior was bilinear, elastic-plastic, presented in Figure 4.2. The elastic range ends at approximately 0.5% strain. While the laminate supported load to approximately 1.8% strain, the allowable was set at 1.0% strain which corresponds to first discontinuous increase in the strain. Shear behavior, Figure 4.4, was linear elastic until approximately 1.0% strain. In this range, the shear modulus was representative of the composite. From approximately 1.0-2.0% strain, the shear modulus transitions from the elastic range to the plastic range. Beyond approximately 2.0% strain, the plastic behavior was representative of the matrix.

4.2.2 $15oz/yd^2$ Unidirectional Carbon/Epoxy Laminate Behavior

Test results for the unidirectional carbon/epoxy laminate are presented in Figures 4.5 through 4.8. It exhibited linear elastic behavior to failure in all tests except in-plane shear, presented in Figure 4.8. Shear behavior was similar to that of the $16oz/yd^2$ unidirectional glass/epoxy. It was linear elastic until approximately 1.0% strain. From approximately 1.0-2.0% strain, the shear modulus transitions from the elastic range to the plastic range. Beyond approximately 2.0% strain, the plastic behavior was representative of the matrix. Note that the plastic modulus is equal to that of the glass/epoxy, substantiating that it is representative of the matrix.

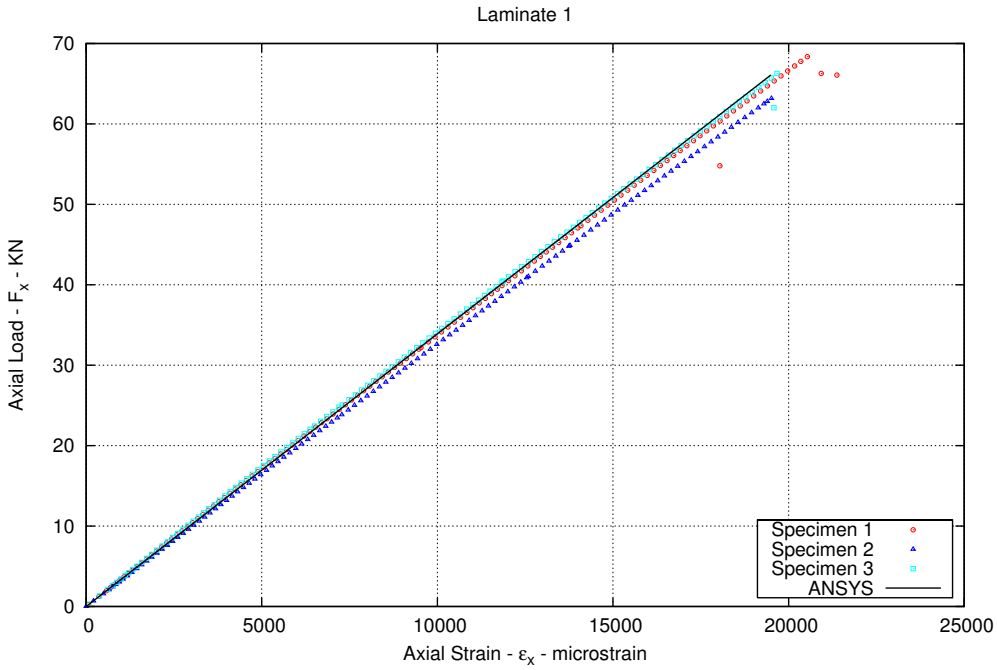

Figure 4.1: Response of the $16oz/yd^2$ unidirectional glass/epoxy laminate to axial tension

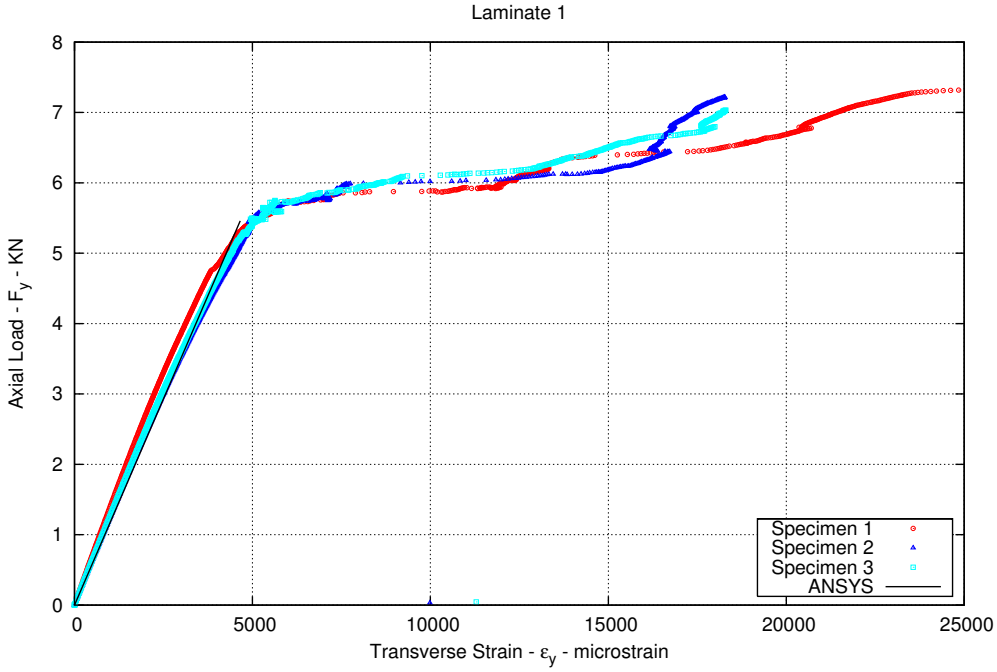

Figure 4.2: Response of the $16oz/yd^2$ unidirectional glass/epoxy laminate to transverse tension

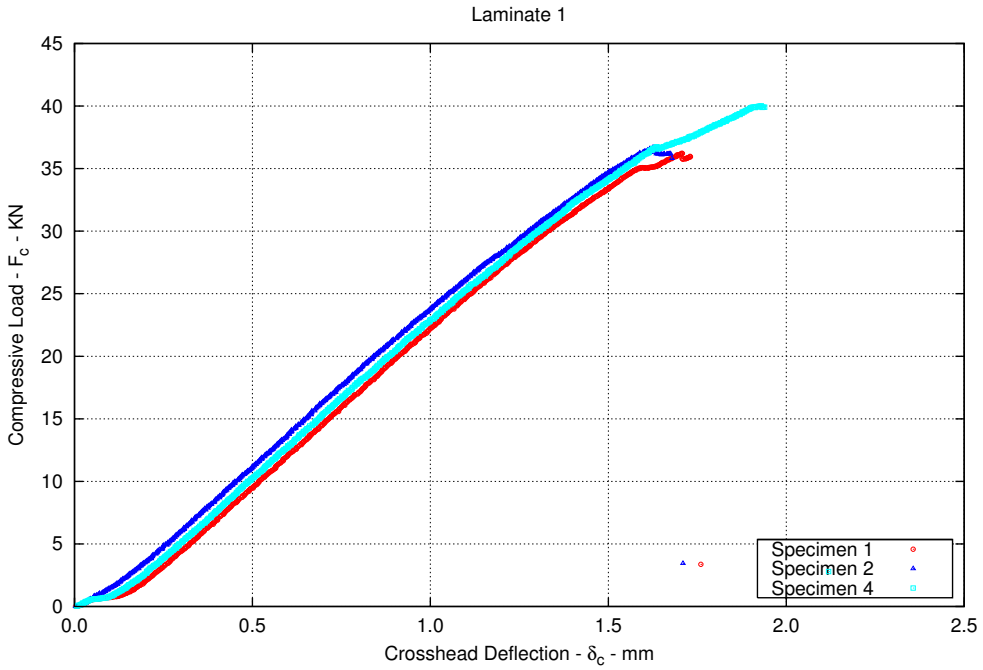

Figure 4.3: Response of the $16oz/yd^2$ unidirectional glass/epoxy laminate to compressive loading

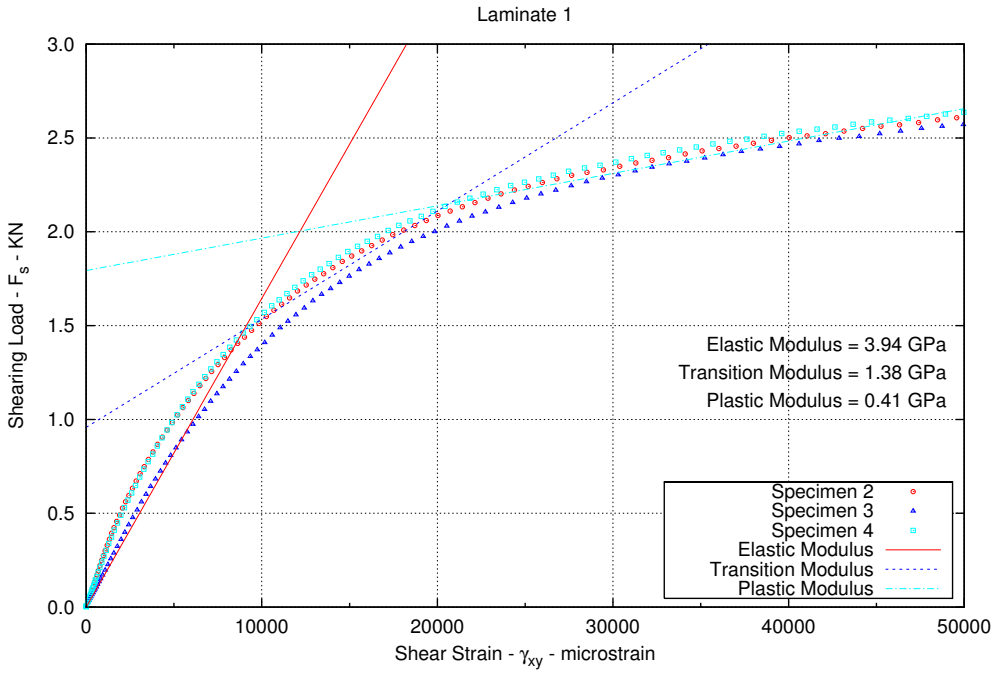

Figure 4.4: Response of the $16oz/yd^2$ unidirectional glass/epoxy laminate to in-plane shear loading

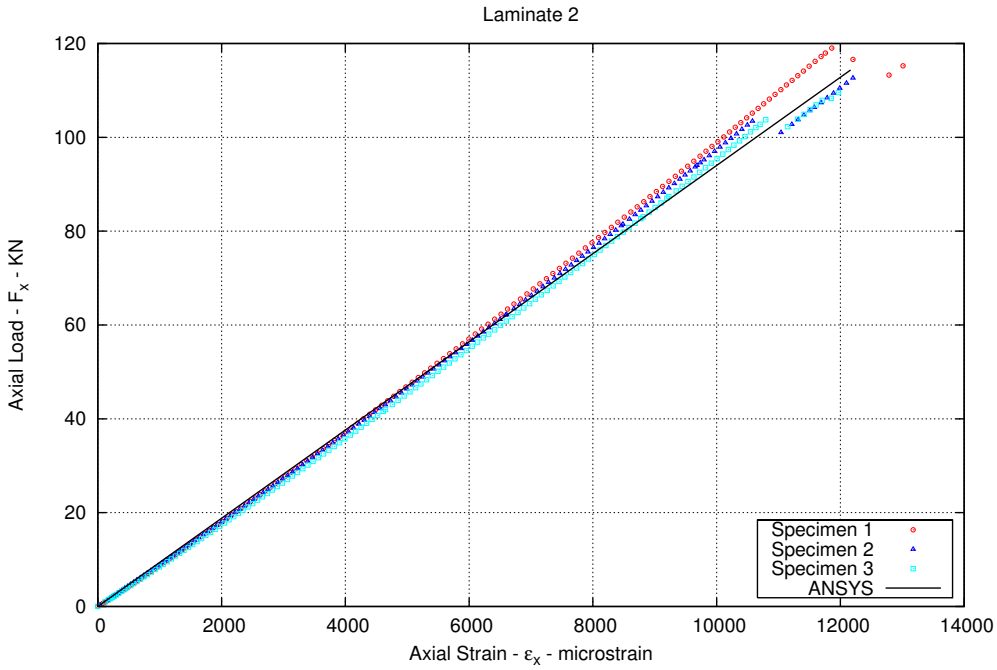

Figure 4.5: Response of the $15oz/yd^2$ unidirectional carbon/epoxy laminate to axial tension

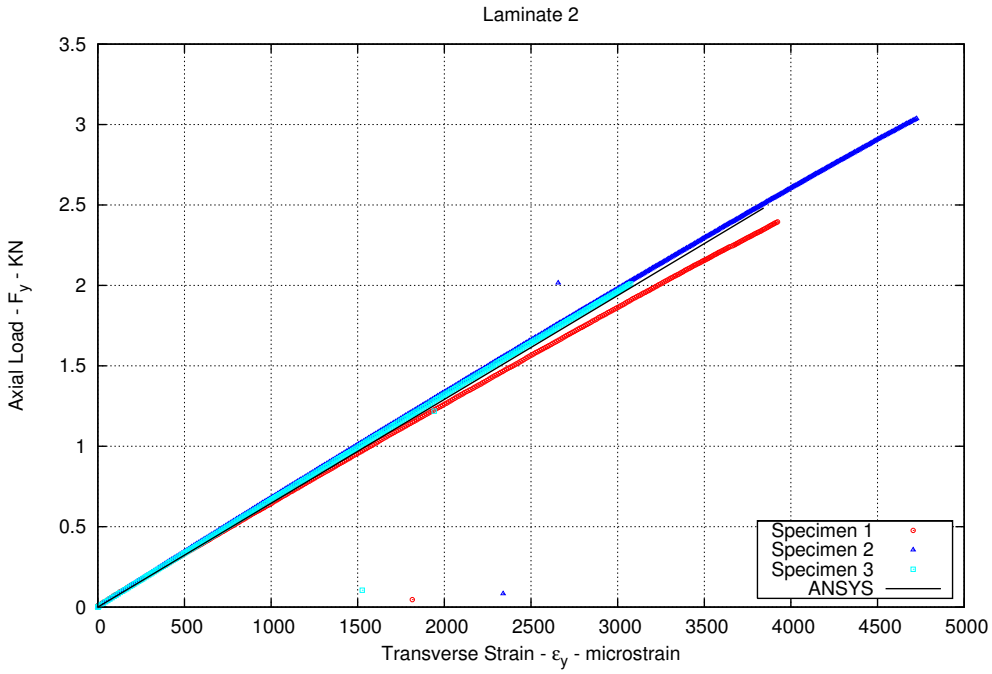

Figure 4.6: Response of the $15oz/yd^2$ unidirectional carbon/epoxy laminate to transverse tension

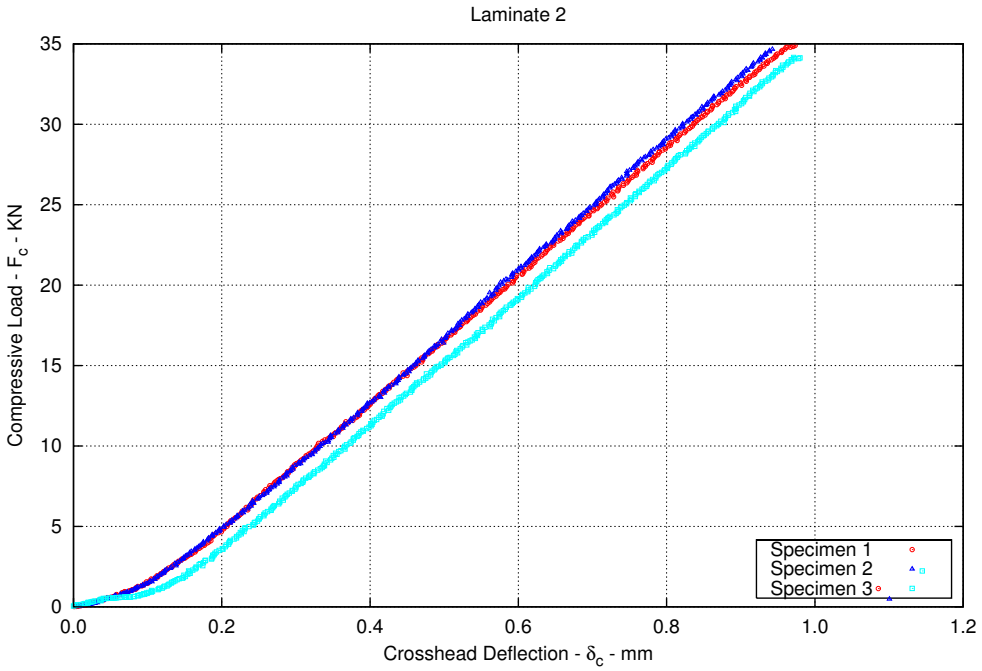

Figure 4.7: Response of the $15oz/yd^2$ unidirectional carbon/epoxy laminate to compressive loading

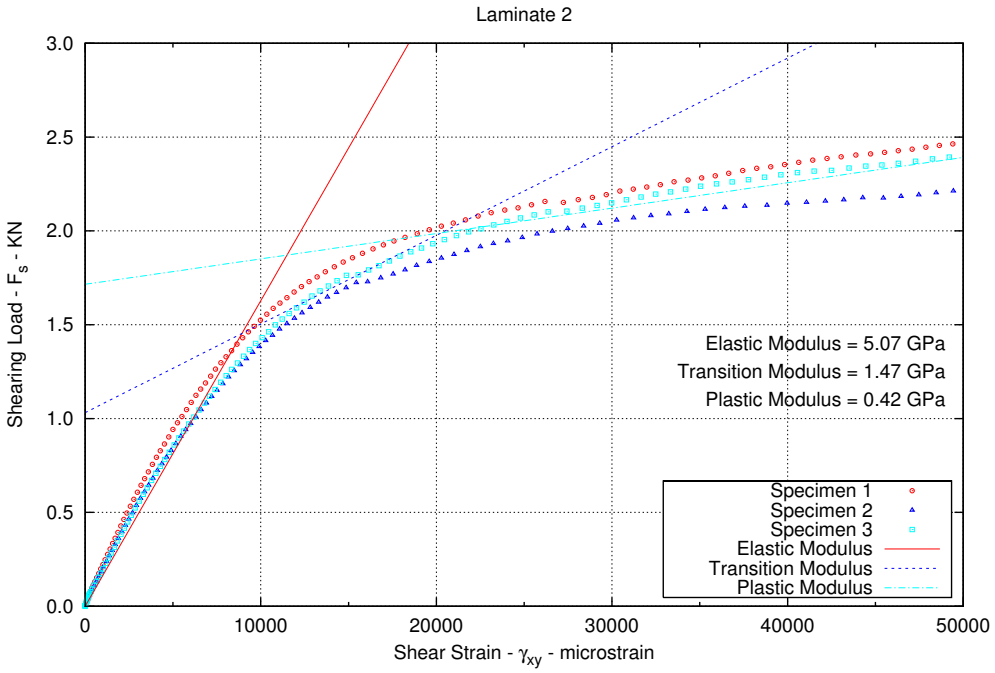

Figure 4.8: Response of the $15oz/yd^2$ unidirectional carbon/epoxy laminate to in-plane shear loading

4.2.3 $12oz/yd^2$ Double Bias Glass/Epoxy Laminate Behavior

Test results for the $12oz/yd^2$ double bias glass/epoxy laminate are presented in Figures 4.9 through 4.11. The response to tension loading, Figure 4.9, was similar to the in-plane shear behavior of the unidirectional composites. Conversely, the in-plane shear response of the double bias glass/epoxy laminate, Figure 4.11, exhibited behavior similar to the tension response of the unidirectional laminates. Compression testing of this material was omitted, as noted in Section 3.2.

4.2.4 $38oz/yd^2$ Double Bias Glass/Epoxy Laminate Behavior

Test results for the $38oz/yd^2$ double bias glass/epoxy laminate are presented in Figures 4.12 through 4.15. The response of the $38oz/yd^2$ double bias glass/epoxy laminate to tension loading, Figure 4.12, was similar to the in-plane shear behavior of the unidirectional composites. Conversely, the in-plane shear response of the laminate, Figure 4.15, exhibited behavior similar to the tension response of the unidirectional laminates.

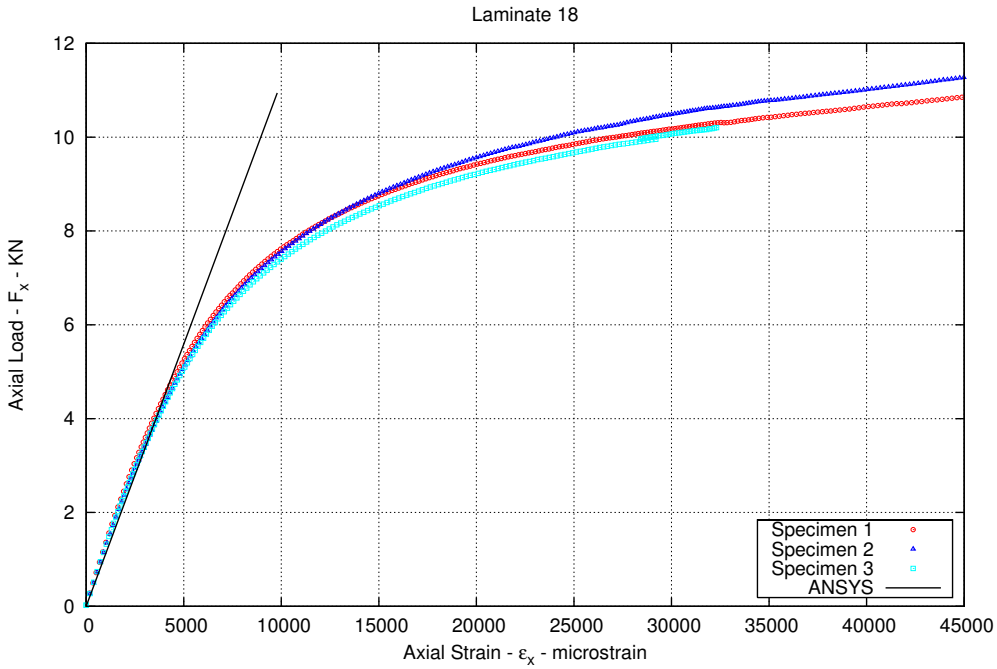

Figure 4.9: Response of the $12oz/yd^2$ double bias glass/epoxy laminate to axial tension

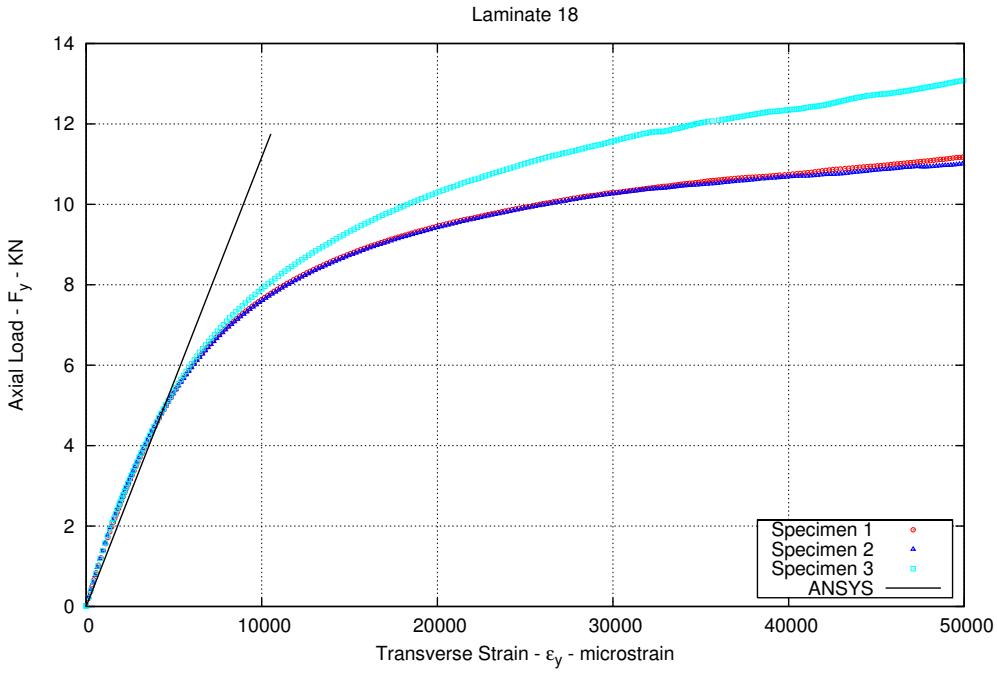

Figure 4.10: Response of the $12oz/yd^2$ double bias glass/epoxy laminate to transverse tension

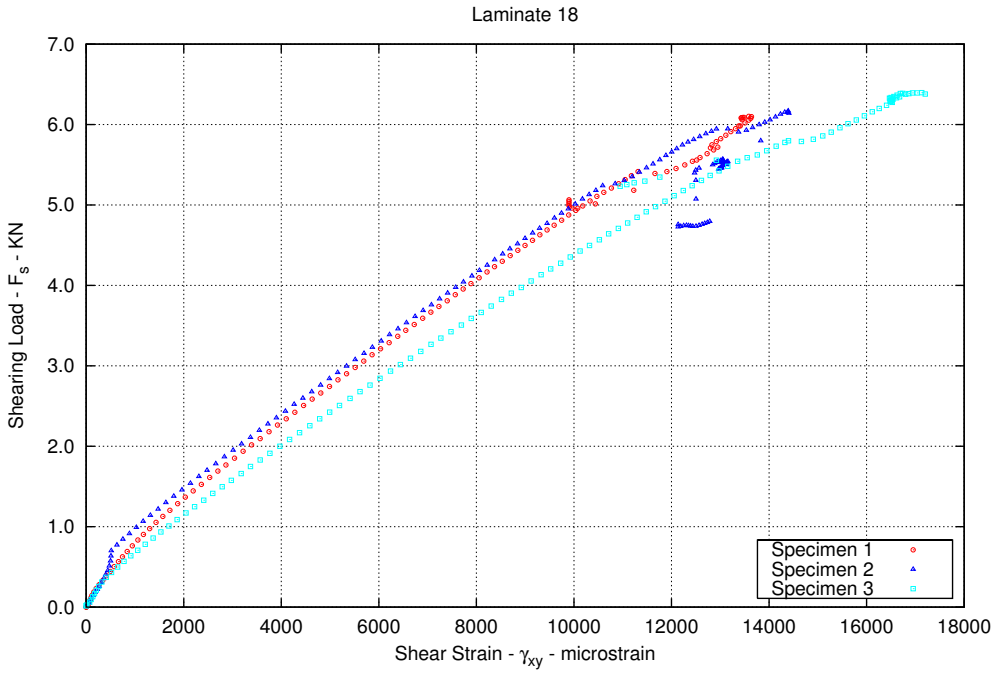

Figure 4.11: Response of the $12oz/yd^2$ double bias glass/epoxy laminate to in-plane shear loading

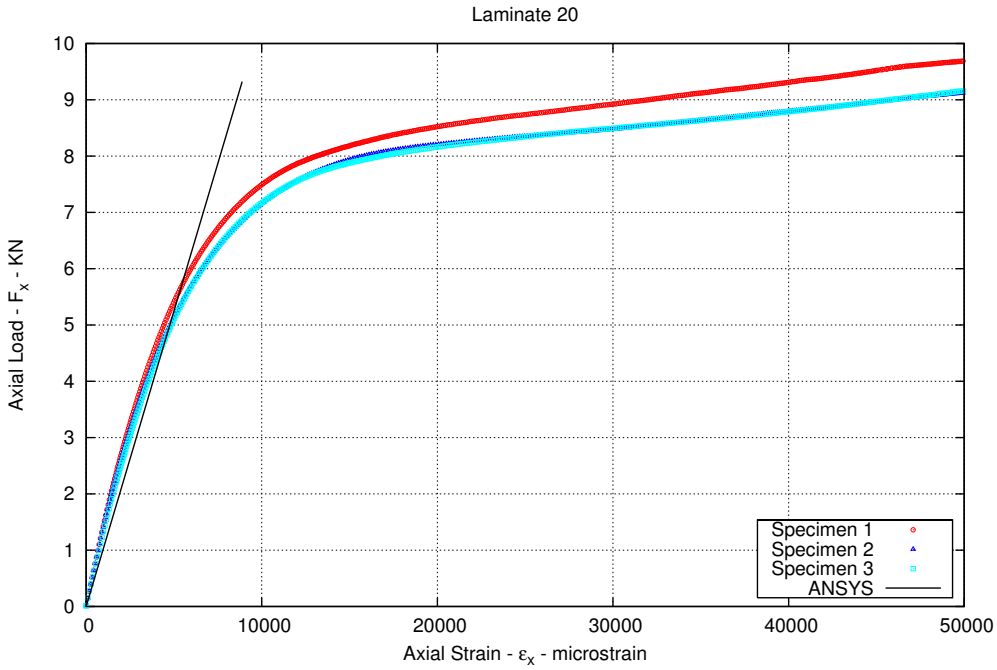

Figure 4.12: Response of the $38oz/yd^2$ double bias glass/epoxy laminate to axial tension

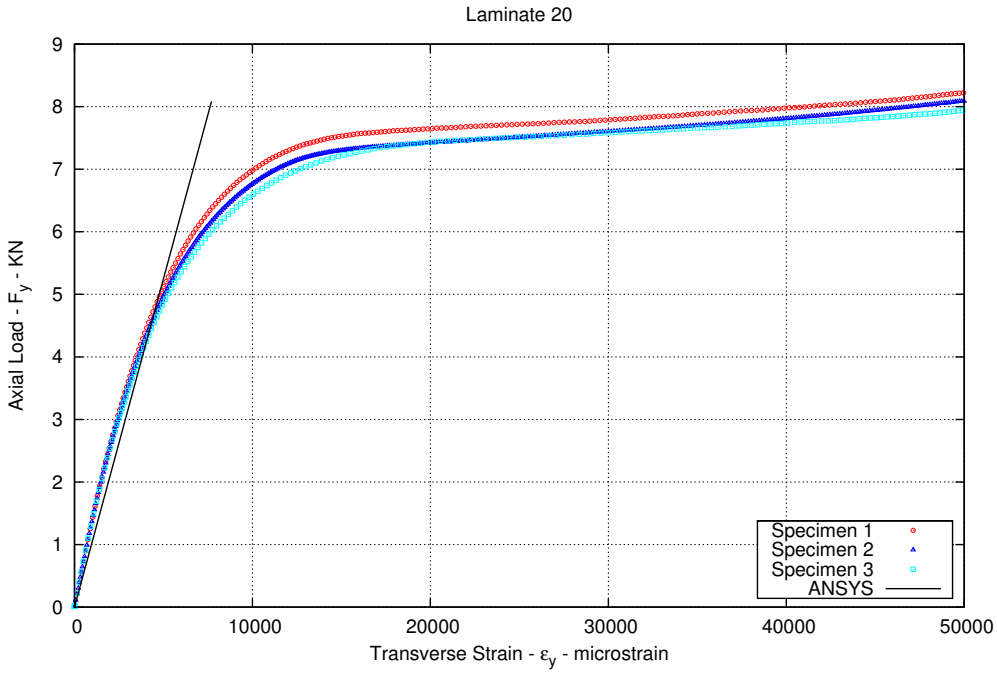

Figure 4.13: Response of the $38oz/yd^2$ double bias glass/epoxy laminate to transverse tension

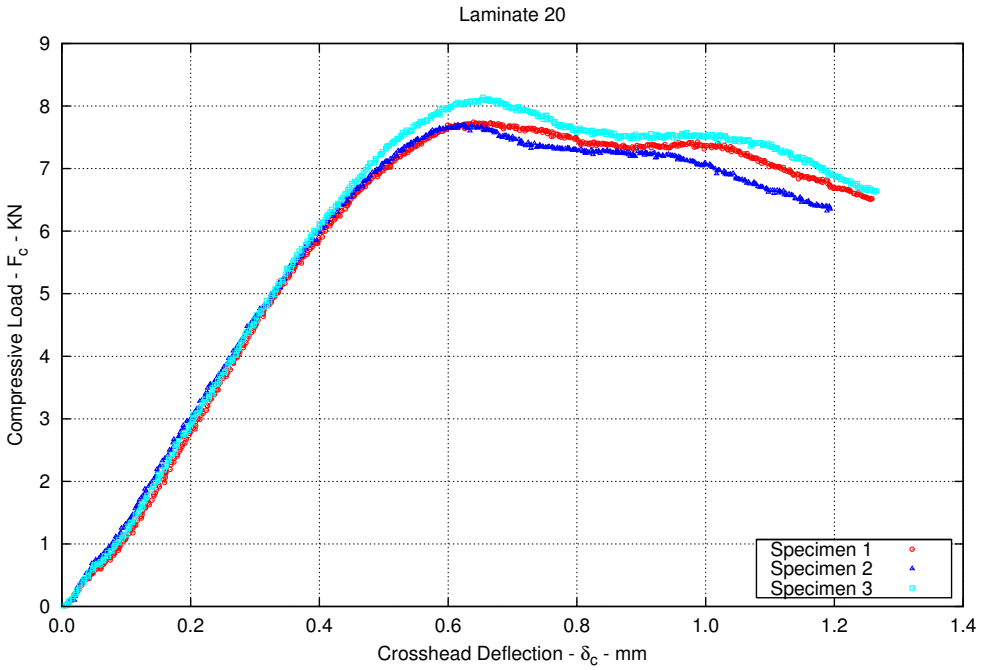

Figure 4.14: Response of the $38oz/yd^2$ double bias glass/epoxy laminate to compressive loading

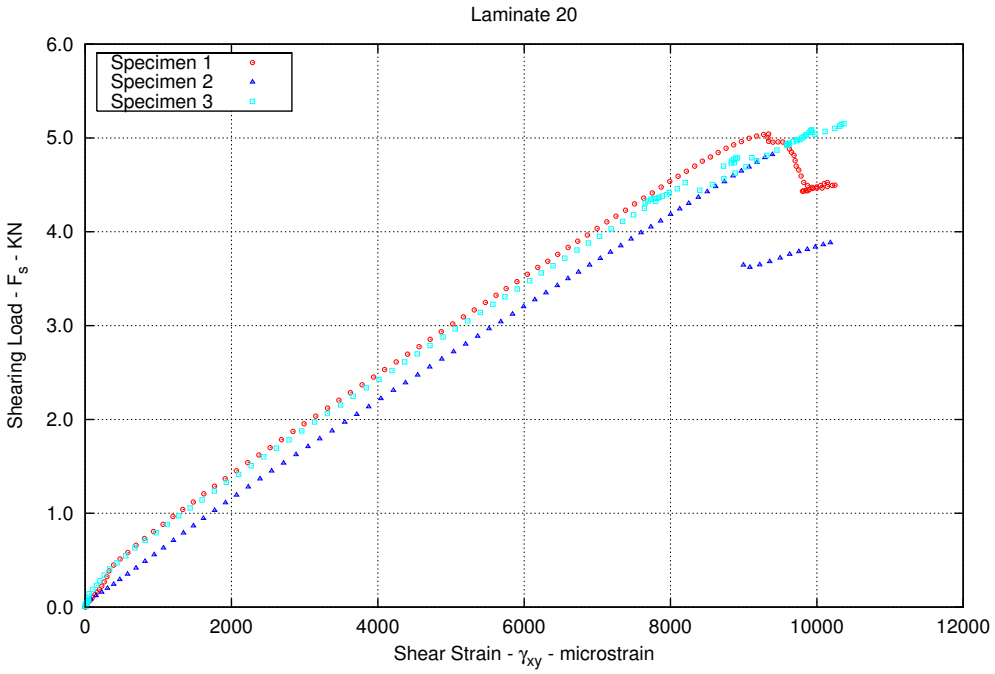

Figure 4.15: Response of the $38oz/yd^2$ double bias glass/epoxy laminate to in-plane shear loading

4.3 Influence of End Constraints on Anisotropic Properties

End constraints can affect measured properties of anisotropic laminates by inducing shearing forces and bending couples at the ends of the specimen.[10–13] Corrections to the apparent moduli due to end constraints can be performed as described in Pindera and Herakovich.[12] The difference between the apparent modulus, E'_x, that is measured in the test and the actual modulus, E_x, can be approximated by Equation 4.1.[12] This correction was formulated for the average stress and to account for contraction of the specimen in the grips due to Poisson's ratio effects. The η term, Equation 4.3, is a measure of the error in the apparent modulus. This term is inversely proportional to the aspect ratio, l/h, of the test specimen. Therefore, the effect of end constraints on the modulus will decrease with increasing aspect ratio. The aspect ratio of the tensile specimens gauge section was 6.

$$E'_x = \frac{1}{S_{11}} \left(\frac{1 - \frac{2}{3}\eta}{1 - \eta} \right) \tag{4.1}$$

where:

$$E_x = \frac{1}{S_{11}} \tag{4.2}$$

$$\eta = \frac{3S_{16}^2}{S_{11}\left(3S_{66} + 2S_{11}\frac{l^2}{h^2}\right)} \tag{4.3}$$

The full compliance matrix of the laminates was not obtained from testing, because the number of strain measurements recorded was insufficient to fully populate the matrix. An estimate of the error, though, can be made utilizing the constitutive properties to calculate the compliance matrix $[S]$ from classical lamination theory (CLT). The results of this calculation are presented in Table 4.3. Correction values in Table 4.3 are calculated from the terms in parenthesis in Equation 4.1. Note that Equation 4.1 corrects for extension/shear coupling and therefore does not fully correct for the extension/shear/bend coupling of laminates 8 and 9.

From the corrections listed in Table 4.3, the apparent modulus from experiment will be greater than the actual modulus of the laminate. For the modulus in the axial direction, E_x, the maximum increase was approximately 3%.

There was no predicted correction to the modulus in the transverse direction, E_y. This is compatible with Rizzo's observation on the effect of the off-axis angle on the shear coupling ratio, S_{16}/S_{XX}.[14] For off-axis angles of 60° - 90°, the shear coupling ratio was approximately 0. Laminates 5 through 9 have varying numbers of lamina at 20°, which would be equivalent to 70° for the tension tests of the laminates in the transverse direction.

The moduli calculated from classical lamination theory are compared against the apparent moduli obtained from testing in Figure 4.16 - 4.18. The standard deviation in the experimental data is plotted with errors bars. The moduli generally correlate with experiment. The CLT value of E_x for laminate 5 exceeds the value from experiment, counter to the error estimated by Equation 4.1. This indicates that the error between CLT and experiment must be attributed to factors other than end constraints. Considering the estimated error in Table 4.3 and the error between CLT and experiment observed in Figure 4.16, factors other than end constraints were dominant for the tensile moduli. Those factors include variance in material, fabrication and testing. For laminates 8 and 9, the apparent tensile moduli are both lower than the modulus from CLT. This suggests that corrections for end constraint of the laminate bending must be performed. In-plane shear modulus, G_{xy}, Figure 4.18, estimated from CLT generally correlates with the modulus from experiment.

Table 4.3: Estimated correction in the modulus based on CLT.

	E_x		E_y	
Laminate	η	Correction	η	Correction
5	0.023	1.008	0.000	1.000
6	0.028	1.010	0.000	1.000
7	0.056	1.020	0.001	1.000
8	0.072	1.026	0.000	1.000
9	0.077	1.028	0.000	1.000
10	0.046	1.016	0.000	1.000
11	0.059	1.021	0.000	1.000
12	0.044	1.016	0.000	1.000
13	0.060	1.021	0.000	1.000
14	0.000	1.000	0.000	1.000
15	0.067	1.024	0.000	1.000
16	0.072	1.026	0.000	1.000

The largest errors in moduli are observed in laminate 21. Laminate 21 is 8 layers of $15oz/yd^2$ unidirectional carbon at $\pm 45°$. Experimental data for laminate 21 is presented in section A.20. The error in axial modulus is approximately 3.5-GPa. In-plane shear modulus calculated with CLT for laminate 21 is nearly a factor of 2 larger than measured in experiment. The source of this discrepancy has not been determined.

4.4 Anisotropic Coupling Properties

The shear coupling ratio, S_{16}/S_{11}, for the anisotropic laminates is plotted in Figure 4.19. Reviewing Table 1.2, laminate 4 can be identified as the uncoupled basis laminate against which to compare laminates 5 through 12 which have varying amounts of off-axis layers. The level of coupling achievable by rotating the glass skins of the laminates is demonstrated by laminates 13 through 16.

The effect of varying the number of off-axis layers and type of axial layers is illustrated by reviewing laminates 4 through 9 which have varying numbers of off-axis carbon layers at 20° and either carbon or glass core. The 4 core layers of 0° carbon in laminate 5 are replaced by 5 layers of 0° glass in laminate 6. This results in a negligible increase in the shear coupling ratio and a substantial decrease in the axial stiffness, E_x(Table 4.4). In laminate 7, 2 of the core layers of 0° carbon in laminate 5 are rotated to 20° resulting in approximately a 50% increase in shear coupling ratio with an approximately 40% decrease in axial stiffness. Laminate 9 is identical to laminate 8 with the exception of layer 4, which is 0° carbon in laminate 8 and glass in laminate 9. This substitution of glass for carbon results in a negligible increase in shear coupling ratio and an approximately 35% decrease in axial stiffness.

The effect of varying the angle of the off-axis plies while keeping the number of angle plies constant is illustrated by studying, in this order, laminates 4, 10, 11, 7 and 12. Four layers are oriented off-axis 10° in laminate 10, 15° in laminate 11, 20° in laminate 7 and 25° in laminate 12. With increasing angle, there is an increase in reduction of the axial stiffness. The shear coupling ratio is maximum at 15° in laminate 11 and decreases after that. Laminate 10, with an axial stiffness reduction of 0.86, exhibits a shear coupling ratio approximately equal to laminate 7, which has an axial stiffness reduction of 0.61. A plot of this reduced set of coupling ratios is presented in Figure 4.20.

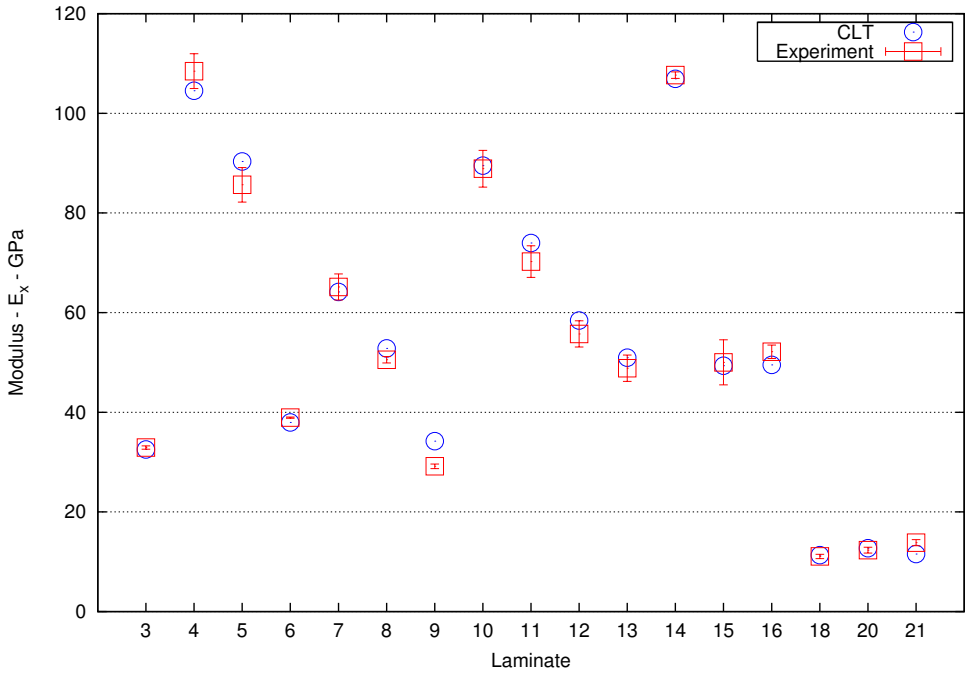

Figure 4.16: Correlation of axial modulus, E_x, from CLT with experiment.

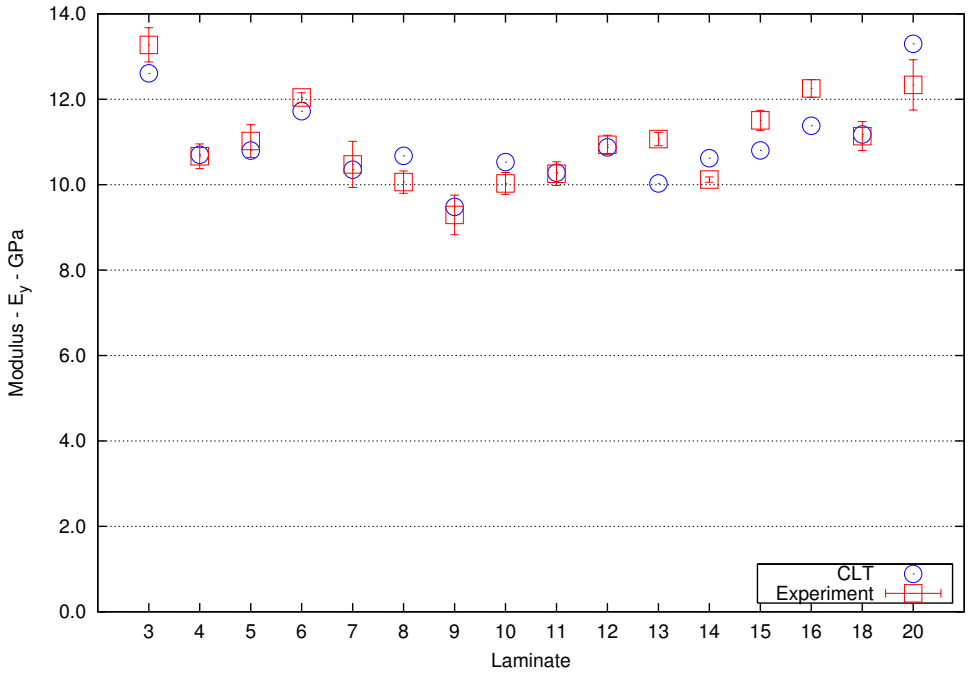

Figure 4.17: Correlation of transverse modulus, E_y, from CLT with experiment.

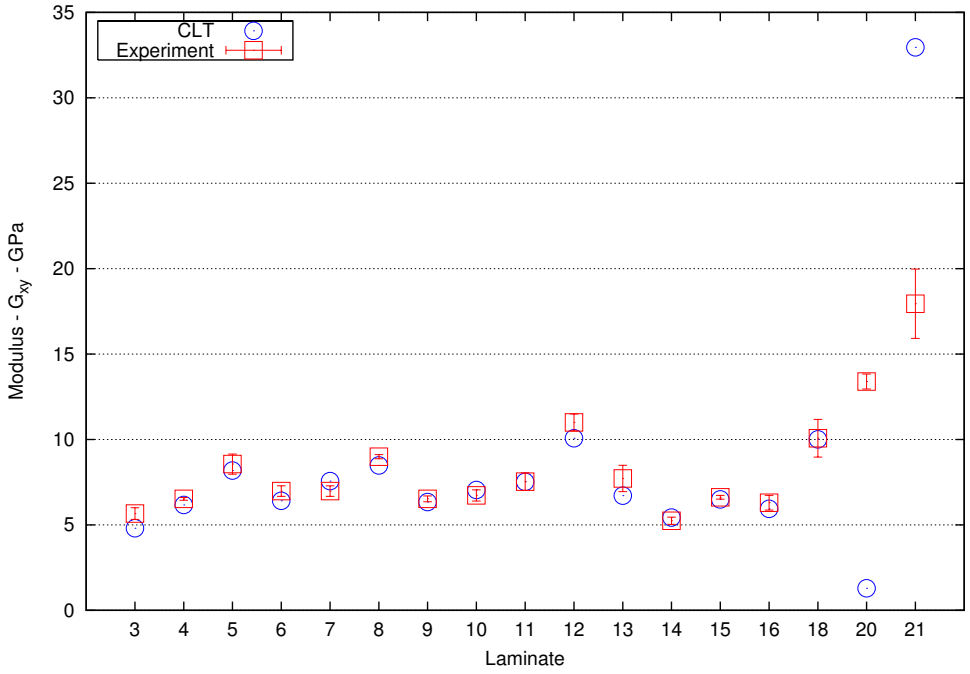

Figure 4.18: Correlation of axial modulus, G_{xy}, from CLT with experiment.

Table 4.4: Effect of coupling on axial modulus.

Laminate	$\frac{S_{16}}{S_{11}}$	E_x	
		(Msi)	Reduction
4	0.00	15.16	1.00
5	-0.89	13.10	0.86
6	-0.91	5.53	0.36
7	-1.33	9.30	0.61
8	-1.48	7.66	0.51
9	-1.50	4.96	0.33
10	-1.30	12.98	0.86
11	-1.42	10.73	0.71
12	-1.15	8.47	0.56
13	-1.37	7.39	—
14	-0.15	15.51	—
15	-1.45	7.15	—
16	-1.53	7.18	—

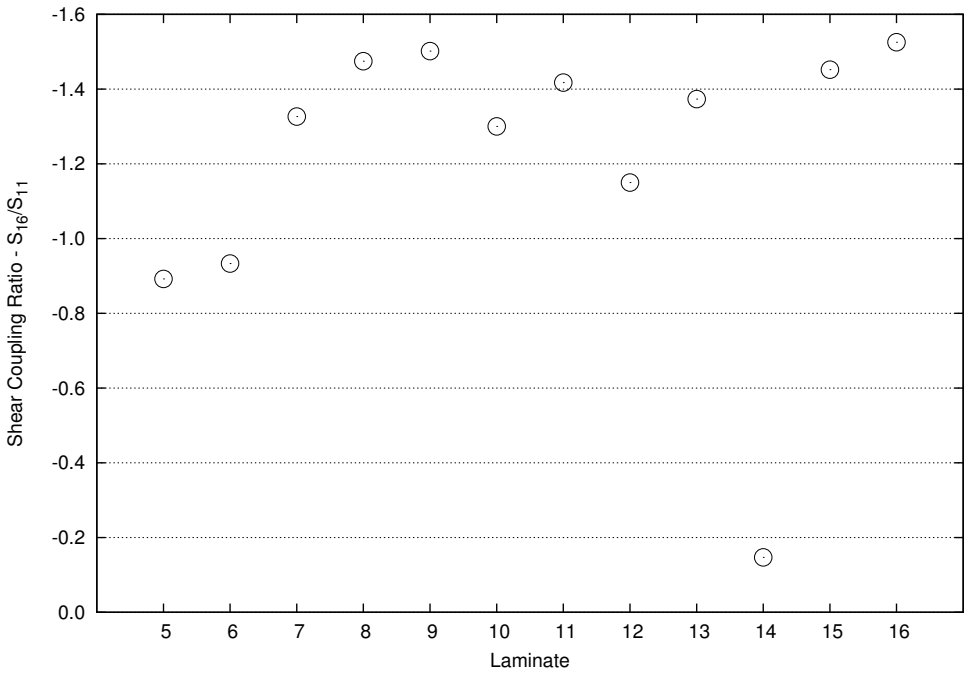

Figure 4.19: Level of coupling in the anisotropic laminates.

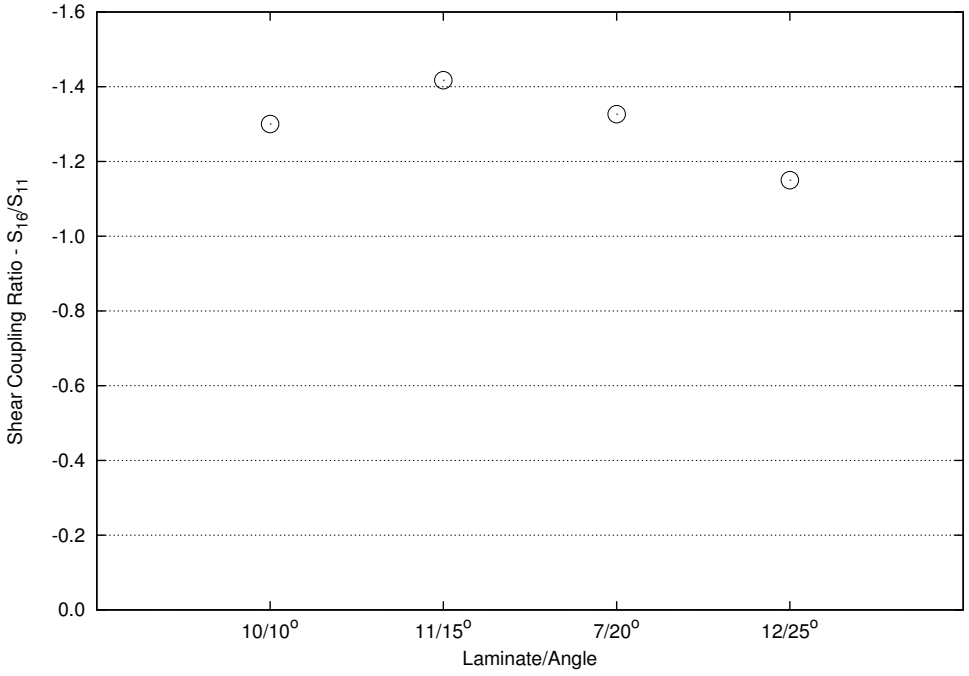

Figure 4.20: Effect of the angle of the off-axis plies on the level of coupling.

4.5 Linear First Ply Failure Analysis

Two aspects of the laminates tested in this study prompted a linear first ply failure analysis. Thirteen of the laminates were hybrid carbon/glass laminates and twelve of the laminates were anisotropic. The analysis was performed to provide insight into which of these factors, in addition to the nonlinear material behavior and end constraint effects, was dominant and how that would affect use of the allowables.

The analysis was performed for the tension and compression tests. ANSYS[15] was utilized for the analysis. The laminates were modeled with the SHELL91 element, an 8-node nonlinear, layered element that supports plasticity and large-strain. Double bias glass epoxy was modeled as one layer. Three failure criteria are defined in ANSYS: max strain, max stress and Tsai-Wu. All three criteria were calculated for each of the laminates. The max strain criteria defines failure as the exceedence of the strain allowables in the principal material directions. Similarly, the max stress criteria defines failure as the exceedence of the strength in the principal material directions. The Tsai-Wu criteria defines a failure surface in stress space which is supposed to account for combined loading conditions.

Boundary conditions were applied to the ends of the model which restrained the model from shearing but allowed contraction due to the effect of Poisson's ratio, noted as $v = 0$ at the center in Figure 4.21. These boundary conditions closely approximated those used in Pagano and Halpin[10] to derive the analytical correction for end constraints. Pagano and Halpin utilized an applied strain as the end loading, while an end stress, σ, was applied to the current analysis. Additionally, the bend coupling in laminates 8 and 9 necessitated constraining the ends from bending and twisting, noted as $w = 0$ and $w_{,x} = 0$ in Figure 4.21. Essentially, this is a clamped condition that allowed contraction due to Poisson's ratio effects. Comparison of this boundary condition with rigid and free boundary conditions is presented in Figure 4.22 for laminate 8 which demonstrated a nonlinear response. Note that the boundary condition utilized in the failure analysis approximates the experimental data better than either the free or rigid boundary condition. Note that the model was restrained from free-body motion in the X direction due to application of equal and opposite stresses at each end.

4.5.1 Axial Tensile Failure

Correlation of the linear first ply failure analysis with experiment for axial tensile loading is presented in Table 4.5 and Figure 4.24. The layer predicted to fail is listed in Table 4.5 for each criteria. For the max strain and max stress criteria, the component of the allowable that was exceeded is listed in addition to the layer.

Estimated failure of the unidirectional laminates was within 2% of the experimental value for all

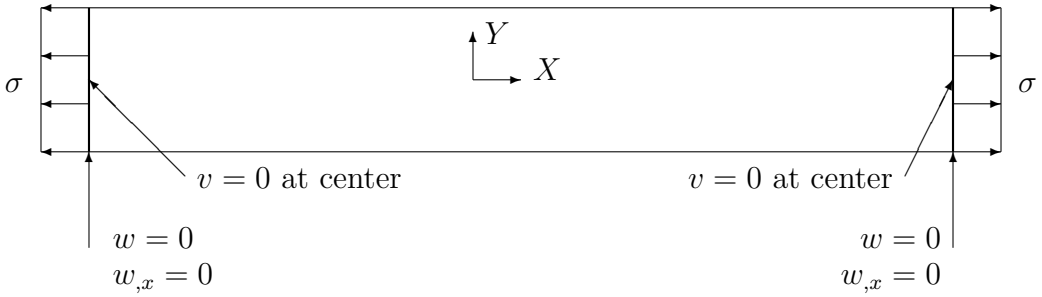

Figure 4.21: Failure analysis boundary condition.

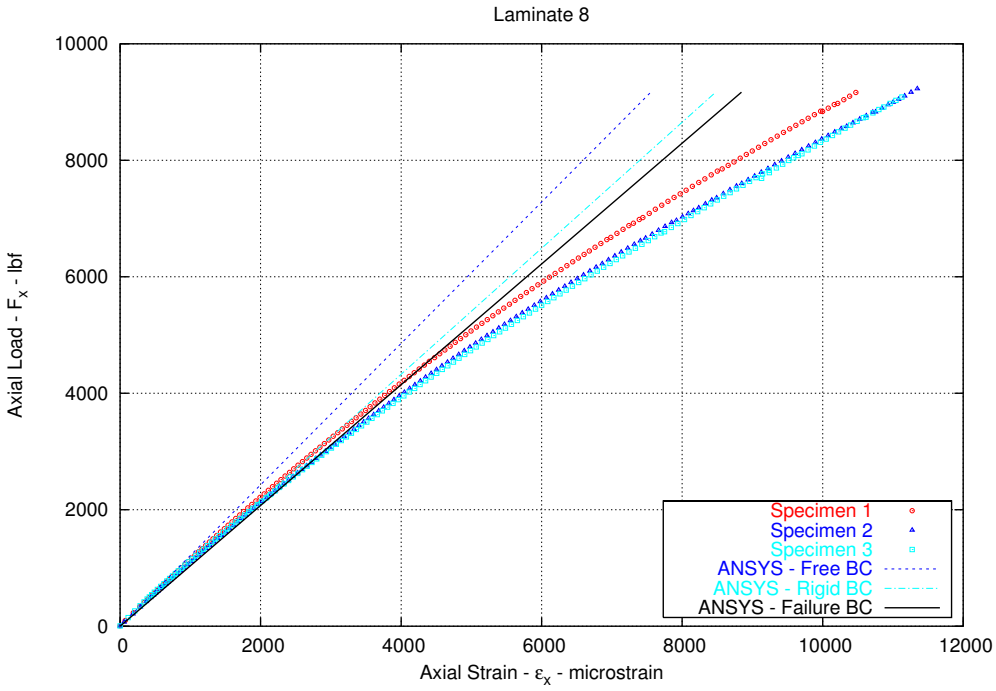

(a) Axial, E_x

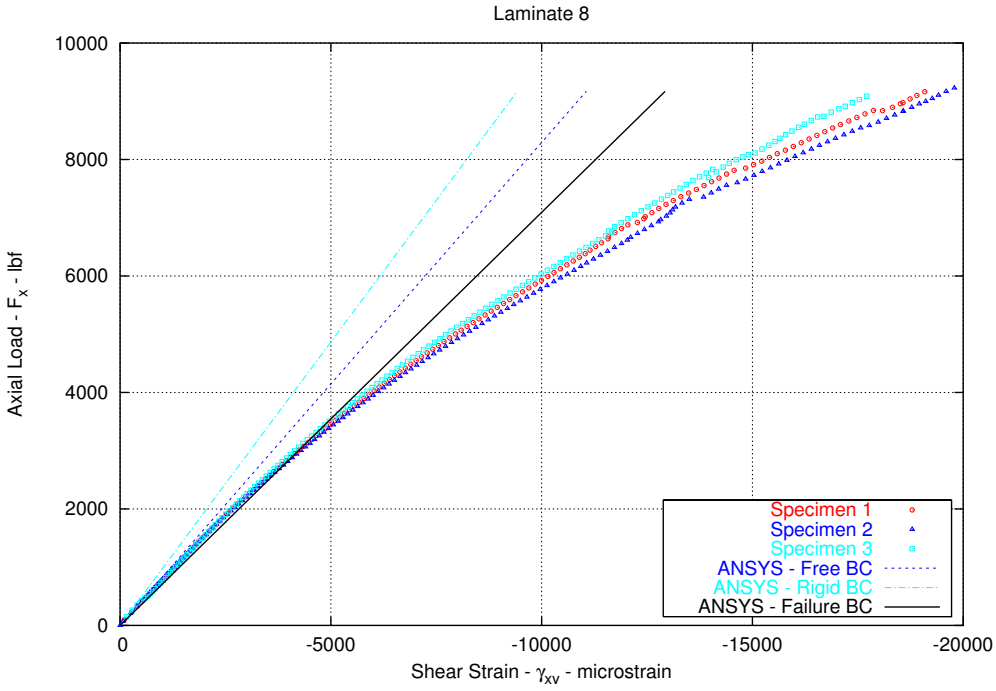

(b) Shear, G_{xy}

Figure 4.22: Effect of boundary conditions on the failure analysis.

criteria. Using the max strain criteria, failure was predicted in the 0° lamina for the uncoupled and least coupled laminates, laminates 3 through 5. Transverse failure was predicted in laminates 13 and 16. Shear failure of the double bias glass skins was predicted for laminates 6 through 12 and 14. The double bias glass responds linearly to shear, Figure 4.11, which supports the max strain failure prediction for the coupled laminates. In addition, failure of the double bias skins was observed in the testing, Figure 4.23. The error in the max strain failure prediction for laminates 18, 20 and 21 was a result of the nonlinear shear-like behavior of those laminates in tension.

The failure predicted by the stressed based criteria was consistently more conservative than max strain. For the uncoupled laminates, the max stress criteria was more conservative than Tsai-Wu. As coupling increased, the Tsai-Wu criteria became increasingly more conservative than max stress. This trend was also observed in a comparison of failure criteria by Soden, Hinton and Kaddour.[16]

In general, failure predicted with the stress based criteria was a result of exceeding shear allowables. A result of this was that the stress based criteria more accurately captured the failure of laminates 18, 20 and 21 than the max strain criteria. The layers and components of failure predicted with max stress correspond to constitutive lamina directions that respond nonlinearly, either the double bias glass or the off-axis carbon. Employing a nonlinear material model should improve the correlation with experiment of all of the criteria.

4.5.2 Transverse Tensile Failure

Correlation of the linear first ply failure analysis with experiment for transverse tensile loading is presented in Table 4.6 and Figure 4.25. The layer predicted to fail is listed in Table 4.6 for each criteria. For the max strain and max stress criteria, the component of the allowable that was exceeded is listed in addition to the layer.

In general, the same failure was predicted with the strain and stress based criteria. The predictions were conservative and consistently a result of matrix failure. The error in the failure predicted with max strain for laminates 1, 3, 18 and 21 was a result of the nonlinear behavior of those laminates. For laminates 1 and 3, the bilinear behavior of the $16oz/yd^2$ unidirectional glass was not captured by the max strain criteria. For laminates 18 and 20, the nonlinear shear-like response was not captured.

4.5.3 Compressive Failure

Correlation of the linear first ply failure analysis with experiment for compressive loading is presented in Table 4.7 and Figure 4.26. As in the case of tension, the layer predicted to fail is listed in Table 4.7 for each criteria. The component of the allowable that was exceeded is listed for max strain and max stress.

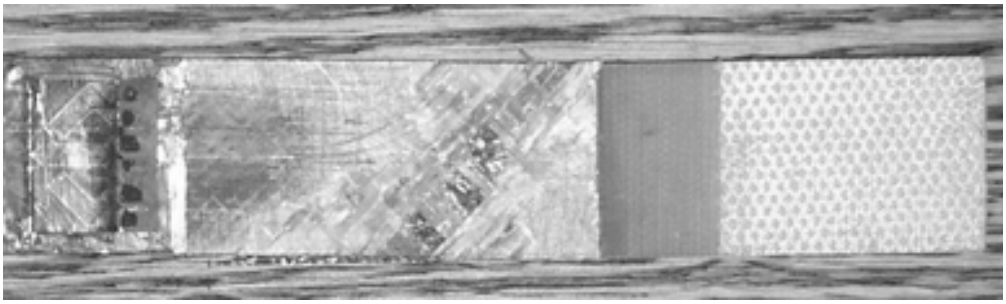

Figure 4.23: Failed laminate 8 tension specimen.

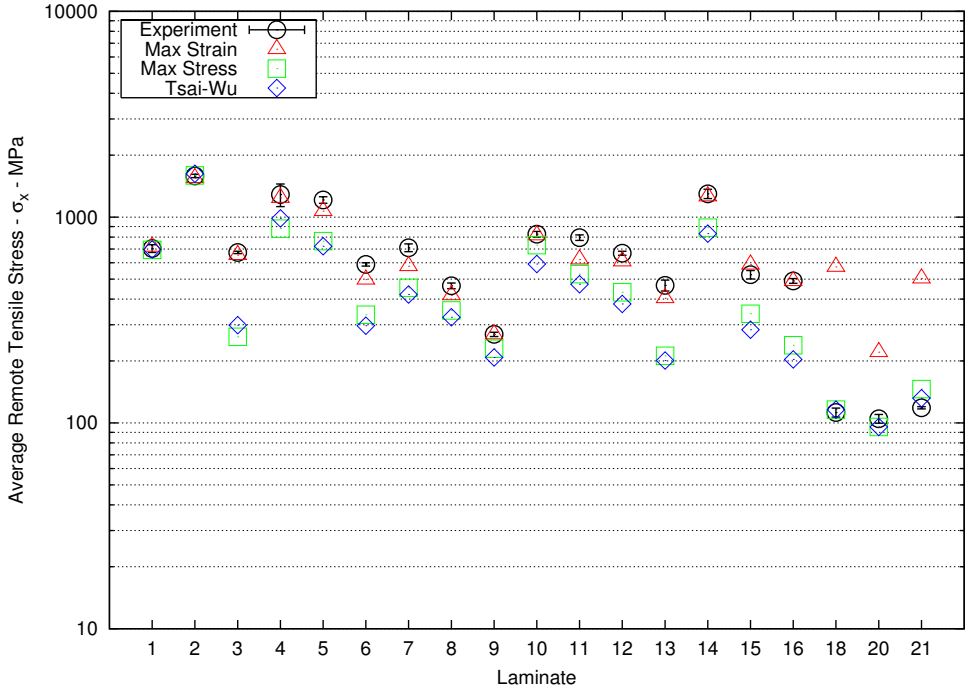

Figure 4.24: Correlation of axial tensile failure analysis with experiment.

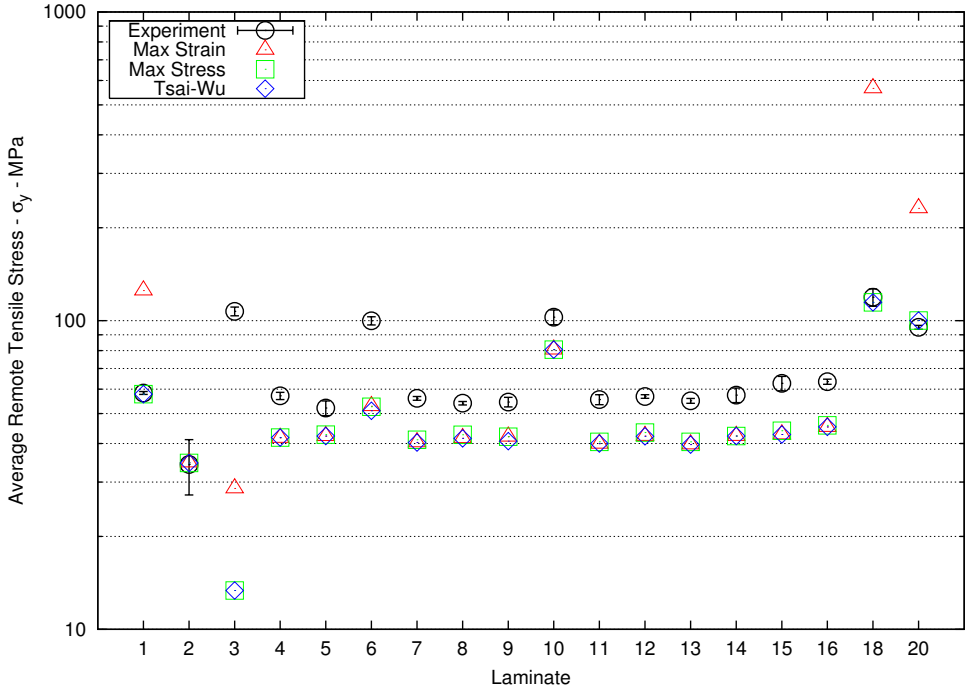

Figure 4.25: Correlation of transverse tensile failure analysis with experiment.

Table 4.5: Axial tensile failure estimates.

	Exp.	Max Strain					Max Stress					Tsai-Wu			
Laminate	(ksi)	Layer	Mat.	Component	(ksi)	% of Exp.	Layer	Mat.	Component	(ksi)	% of Exp.	Layer	Mat.	(ksi)	% of Exp.
1	704	1	0G	X	717	102%	1	0G	X	694	99%	1	0G	696	99%
2	1,585	1	0C	X	1,546	98%	1	0C	X	1,595	101%	1	0C	1,624	102%
3	674	2	0G	X	654	97%	1	DB	X	262	39%	1	DB	299	44%
4	1,288	2	0C	X	1,239	96%	1	DB	X	879	68%	1	DB	987	77%
5	1,212	3	0C	X	1,070	88%	2	20C	XY	765	63%	1	DB	722	60%
6	589	1	DB	XY	497	84%	3	20C	XY	335	57%	1	DB	297	50%
7	710	1	DB	XY	577	81%	2	20C	XY	453	64%	2	20C	421	59%
8	464	1	DB	XY	417	90%	2	20C	XY	352	76%	2	20C	326	70%
9	269	1	DB	XY	269	100%	2	20C	XY	229	85%	2	20C	208	77%
10	826	1	DB	XY	814	98%	2	10C	XY	731	88%	1	DB	592	72%
11	795	1	DB	XY	622	78%	2	15C	XY	528	66%	1	DB	472	59%
12	668	1	DB	XY	609	91%	2	25C	XY	431	65%	2	25C	378	57%
13	466	1	75G	Y	404	87%	1	75G	Y	212	46%	1	75G	201	43%
14	1,299	7	DB	XY	1,260	97%	1	DB	XY	888	68%	1	DB	831	64%
15	525	5	0C	X	587	112%	3	20C	XY	339	65%	1	20C	284	54%
16	490	1	90G	Y	488	99%	1	90G	Y	238	48%	1	90G	204	42%
18	112	1	DB	X	573	510%	1	DB	X	116	103%	1	DB	116	103%
20	105	1	DB	Y	220	211%	1	DB	X	96	91%	1	DB	96	91%
21	118	1	45C	XY	503	425%	1	45C	XY	146	123%	1	45C	132	111%

DB	± 45 $12 oz/yd^2$ double bias glass	10C	$10°$ $15 oz/yd^2$ unidirectional carbon
0G	$0°$ $16 oz/yd^2$ unidirectional glass	15C	$15°$ $15 oz/yd^2$ unidirectional carbon
75G	$75°$ $6 oz/yd^2$ unidirectional glass	20C	$20°$ $15 oz/yd^2$ unidirectional carbon
90G	$90°$ $6 oz/yd^2$ unidirectional glass	25C	$25°$ $15 oz/yd^2$ unidirectional carbon
0C	$0°$ $15 oz/yd^2$ unidirectional carbon	45C	$45°$ $15 oz/yd^2$ unidirectional carbon

Table 4.6: Transverse tensile failure estimates.

	Exp.	Max Strain					Max Stress					Tsai-Wu			
Laminate	(ksi)	Layer	Mat.	Component	(ksi)	% of Exp.	Layer	Mat.	Component	(ksi)	% of Exp.	Layer	Mat.	(ksi)	% of Exp.
1	58	1	0G	Y	125	215%	1	0G	Y	58	99%	1	0G	58	99%
2	34	1	0C	Y	35	101%	1	0C	Y	35	101%	1	0C	35	101%
3	107	2	0G	Y	127	119%	2	0G	Y	59	55%	2	0G	59	12%
4	57	2	0C	Y	42	73%	2	0C	Y	42	73%	2	0C	42	73%
5	52	3	0C	Y	42	81%	3	0C	Y	43	82%	3	0C	42	81%
6	100	3	20C	Y	53	53%	3	20C	Y	53	53%	3	20C	51	51%
7	56	4	0C	Y	40	72%	4	0C	Y	41	73%	4	0C	40	72%
8	54	5	20C	Y	42	77%	5	20C	Y	43	79%	5	20C	42	77%
9	54	2	20C	Y	42	77%	2	20C	Y	42	77%	2	20C	41	75%
10	103	4	0C	Y	81	79%	4	0C	Y	81	79%	4	0C	81	79%
11	55	4	0C	Y	40	72%	4	0C	Y	40	73%	4	0C	40	72%
12	57	4	0C	Y	42	74%	4	0C	Y	43	76%	4	0C	42	74%
13	55	5	0C	Y	40	72%	5	0C	Y	40	74%	5	0C	40	72%
14	57	2	0C	Y	42	74%	2	0C	Y	42	74%	7	0C	42	74%
15	63	5	0C	Y	43	68%	5	0C	Y	44	70%	5	0C	43	68%
16	63	5	0C	Y	45	71%	5	0C	Y	46	72%	5	0C	45	71%
18	119	1	DB	Y	565	475%	1	DB	Y	115	96%	1	DB	115	96%
20	95	1	DB	Y	231	243%	1	DB	Y	100	105%	1	DB	100	105%

0G $0°$ $16oz/yd^2$ unidirectional glass
0C $0°$ $15oz/yd^2$ unidirectional carbon
20C $20°$ $15oz/yd^2$ unidirectional carbon
DB ± 45 $12oz/yd^2$ double bias glass

Estimated failure of the unidirectional laminates correlated well with experiment, within 5% for all failure criteria. With the exception of max strain failure of laminate 9, compressive failure was due to carbon in laminates 4 through 16 for all criteria. The same compressive failure was obtained with max strain and max stress for most laminates. For laminates 5, 7, 11, 12 and 15, the transverse component of failure was predicted by the max strain criteria. This suggests expansion of the double bias skins due to Poisson's ratio exceeded the transverse limit of the carbon layers. As in the case of tension, the max strain criteria did not accurately capture the behavior of laminate 21.

Tsai-Wu criteria consistently predicted the most conservative failure stress. The failure predicted by Tsai-Wu was approximately half the value observed in experiment for the coupled laminates. The data requirements for Tsai-Wu exceed those for max strain and max stress. Allowables for transverse compression of the unidirectional laminae were not obtained from testing. Based on representative data in Jones,[17] these compressive allowables were set equal to three times the tension allowable perpendicular to the fibers. No compression allowable data was obtained for the double bias glass lamina. In this case, the compression allowables were set equal to the tension allowables. Clearly, these assumptions have the largest impact on Tsai-Wu criteria and contribute to the lack of correlation between Tsai-Wu and experiment.

A compressive interaction effect of carbon with the double bias glass layers was observed comparing laminates 2 and 4. Laminate 4 was essentially laminate 2 sandwiched between two layers of double bias glass. The experimental compression strength of laminate 4 was greater than laminate 2, while a decrease was observed in the analysis. Furthermore, laminate 4 failed in the experiment at 1.0% strain compared to 0.78% strain for laminate 2. The experimental data indicates that the interaction between the double bias skins and the unidirectional carbon improves the compressive failure of the carbon. This effect was not estimated by the analysis and contradicts results presented by Soutis[18] for T800/924C carbon-fibre/epoxy with a stacking sequence of $[(\pm 45/0_2)_3]_s$. A noted difference between laminate 4 and the laminate study by Soutis is that laminate 4 is a carbon/glass hybrid. Further study into this interaction is required.

Table 4.7: Compressive failure estimates.

	Exp.	Max Strain					Max Stress					Tsai-Wu			
Laminate	(ksi)	Layer	Mat.	Component	(ksi)	% of Exp.	Layer	Mat.	Component	(ksi)	% of Exp.	Layer	Mat.	(ksi)	% of Exp.
1	791	1	0G	X	749	95%	1	0G	X	777	98%	1	0G	776	98%
2	956	1	0C	X	1,005	105%	1	0C	X	970	101%	1	0C	970	101%
3	685	2	0G	X	683	100%	1	DB	X	261	38%	1	DB	297	43%
4	986	2	0C	X	845	86%	2	0C	X	817	83%	2	0C	726	74%
5	827	1	0C	XY	552	67%	1	0C	X	587	71%	1	0C	411	50%
6	551	1	20C	XY	414	75%	1	20C	X	277	50%	1	20C	245	44%
7	544	4	0C	Y	350	64%	2	0C	X	362	67%	4	0C	244	45%
8	397	5	20C	X	264	66%	2	20C	XY	249	63%	5	20C	176	44%
9	330	1	DB	XY	200	60%	2	20C	XY	170	52%	1	20C	156	47%
10	772	4	0C	X	538	70%	4	0C	X	521	67%	4	0C	361	47%
11	614	4	0C	Y	419	68%	2	15C	X	421	68%	4	0C	280	46%
12	521	4	0C	Y	312	60%	3	25C	XY	340	65%	4	0C	226	43%
13	414	5	0C	X	299	72%	3	20C	XY	284	69%	5	0C	207	50%
14	937	7	0C	X	720	77%	7	0C	X	695	74%	7	0C	673	72%
15	386	5	0C	Y	281	73%	3	20C	XY	258	67%	5	0C	183	47%
16	410	5	0C	X	285	70%	3	20C	XY	267	65%	5	0C	215	53%
20	168	1	DB	X	131	78%	1	DB	X	158	94%	1	DB	158	94%
21	181	1	45C	XY	468	259%	1	45C	XY	150	83%	1	45C	161	89%

DB ± 45 $12 oz/yd^2$ double bias glass
0G 0° $16 oz/yd^2$ unidirectional glass
0C 0° $15 oz/yd^2$ unidirectional carbon
45C 45° $15 oz/yd^2$ unidirectional carbon
20C 20° $15 oz/yd^2$ unidirectional carbon
25C 25° $15 oz/yd^2$ unidirectional carbon
15C 15° $15 oz/yd^2$ unidirectional carbon

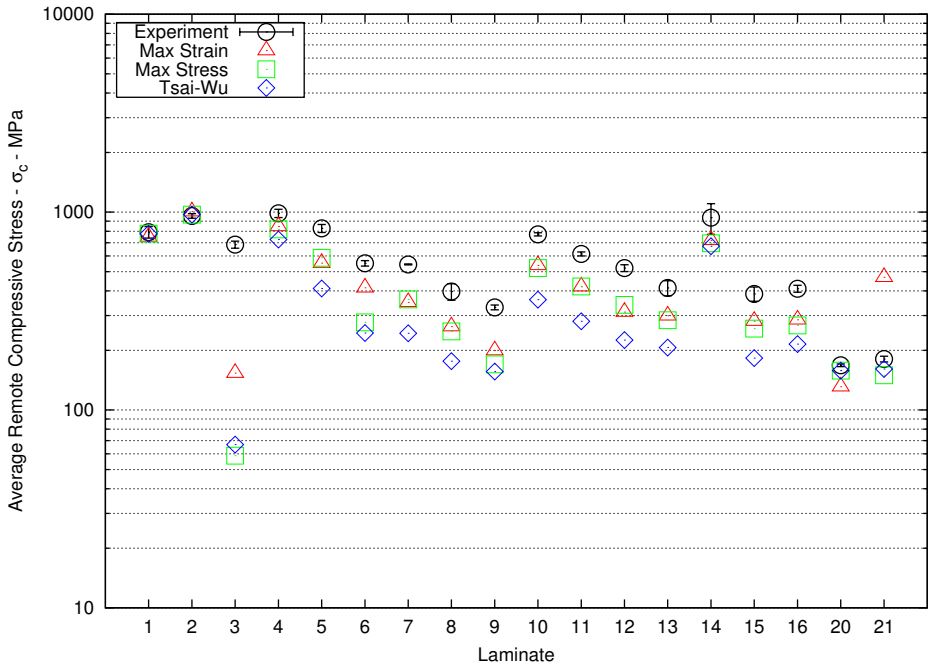

Figure 4.26: Correlation of compressive failure analysis with experiment.

5. Conclusions and Recommendations

The conclusions to be drawn from the testing and analysis reported in the previous sections are:

- Test results for the tensile moduli for all of the anisotropic laminates correlate generally well with those determined using classical lamination theory without further correction for the effects of end constraints imposed by the test fixtures. The coupons used in the present tests exhibited gage aspect ratios of 5:1, and no conclusions can be drawn as to whether end constraints might be significant for shorter coupons.
- Test results for shear moduli for the anisotropic laminates suggest that end constraints are affecting the results.
- The results indicate that extension/shear coupling is maximized with the least loss in axial tensile stiffness by using carbon fibers oriented 15° from the long axis for approximately two-thirds of the laminate volume (discounting skin layers), with reinforcing carbon fibers oriented axially comprising the remaining one-third of the volume.
- First-ply failure predicted by finite element analyses proves generally conservative for all three of the failure criteria examined maximum stress, maximum strain, and Tsai-Wu with the stress-based criteria the most conservative. For laminates that respond nonlinearly to loading, large error is observed in the prediction of failure using maximum strain as the criterion.

Appropriate follow-up to this study would include testing anisotropic laminates in which higher fractions of the fibers are rotated to smaller angles than were studied here. In the present study, the only trade-off of fiber angle is conducted by examining 10°, 15°, 20°, and 25° fibers, all comprising approximately two-thirds of the core laminate (i.e., excluding the biaxial glass skins). Higher concentration of off-axis fibers is examined in Laminate 8, but only with 20° fibers. Therefore, the conclusion that two-thirds of the fibers oriented at 15° provides the best combination of coupling and stiffness is true only within the envelop of laminates studied here. It may be that a higher concentration of fibers turned to 10°, or nearly all of the fibers turned to an even smaller angle might offer a superior combination of coupling and stiffness.

It would also be appropriate to consider further tests to discern the influence of the test fixture end constraints on the in-plane shear modulus and strength measurements. As noted above, the results of the present study suggest the end constraints are significant for shear tests. However, as also noted in the text of the report, an insufficient number of strain measurements (i.e., components of strain) were recorded with each laminate to fully populate the stiffness matrix. In the present study, we have been able to determine whether the stiffness matrix predicted with classical lamination theory does or does not correlate well with the experimental results, which provides an indication of whether end constraint effects are or are not significant for certain tests. However, the methods do not necessarily lend themselves to highly accurate correction of results where end constraint effects are influencing the test results, as is the case for in-plane shear. Therefore, during any follow-on tests, we recommend that all coupons be instrumented with three-element strain rosettes for axial tension, transverse tension, and in-plane shear tests. This would enable fully populating the stiffness matrix and a more accurate correction for end constraint effects.

Finally, recommended follow-up to the first-ply failure analysis would include nonlinear failure analyses. A number of nonlinear failure criteria have been published, and it would be interesting to verify them against the test results for the anisotropic materials examined in the present study. All of the linear failure criteria studied here are conservative because they neglect the nonlinear stress-strain behavior of the materials particularly the ±45° glass and the off-axis fibers near failure. Nonlinear failure criteria would ostensibly be more accurate, albeit at the cost of higher computation time.

Bibliography

[1] Anon., "Standard Test Method for Ignition Loss of Cured Reinforced Plastics," ASTM D 2584–02, 2002.

[2] Anon., "Standard Test Method for Void Content of Reinforced Plastics," ASTM D 2734–94, 1994.

[3] Anon., "Standard Test Methods for Density and Specific Gravity (Relative Density) of Plastics by Displacement," ASTM D792–00, 2000.

[4] Anon., "Standard Test Method for Tensile Properties of Polymer Matrix Composite Materials," ASTM D3039–00, 2000.

[5] Anon., "SACMA Recommended Test Method for Compressive Properties of Oriented Fiber-Resin Composites," SRM 1R-94, 1994.

[6] Anon., "Standard Test Method for Shear Properties of Composite Materials by the V-Notched Beam Method," ASTM D5379–98, 1998.

[7] Anon., "Standard Test Method for Short-Beam Strength of Polymer Matrix Composite Materials and Their Laminates," ASTM D 2344–00, 2000.

[8] Anon., "ARAMIS v 5.3.0 User Manual," Product documentation, GOM, mbH., 2004.

[9] Anon., "Transverse Sensitivity Errors," Micro-measurements tech. note 509, 1982.

[10] Pagano, N. J. and Halpin, J. C., "Influence of End Constraint in the Testing of Anisotropic Bodies," *Journal of Composite Materials*, Vol. 2, No. 1, 1968, pp. 18–31.

[11] Halpin, J. C., Pagano, N. J., Whitney, J. M., and Wu, E. M., "Characterization of Anisotropic Composite Materials," *Composite Materials: Testing and Design*, ASTM, 1969, pp. 37–47.

[12] Pindera, M.-J. and Herakovich, C. T., "Shear Characterization of Unidirectional Composites with the Off-Axis Tension Test," *Experimental Mechanics*, , No. 26, 1986, pp. 103–112.

[13] Nemeth, P., Herakovich, C. T., and Post, D., "On the Off-Axis Tension Test for Unidirectional Composites," *Composites Technology Review*, , No. 5, 1983, pp. 61–68.

[14] Rizzo, R. R., "More on the Influence of End Constraints on Off-Axis Tensile Tests," *Journal of Composite Materials*, Vol. 3, No. 1, 1969, pp. 202–219.

[15] Anon., "ANSYS Release 8.0 Documentation," Product documentation, ANSYS Inc., 2004.

[16] Soden, P. D., Hinton, M. J., and Kaddour, A. S., "A Comparison of the Predictive Capabilities of Current Failure Theories for Composite Laminates," *Composites Science and Technology*, , No. 58, 1998, pp. 1225–1254.

[17] Jones, R. M., *Mechanics of Composite Materials*, Hemisphere Publishing Corporation, 1st ed., 1975.

[18] Soutis, C., "Measurement of the Static Compressive Strength of Carbon-Fibre/Epoxy Laminates," *Composites Science and Technology*, , No. 42, 1991, pp. 373–392.

DISTRIBUTION

James Ahlgrimm
Office of Wind and Hydropower Technologies
EE-2B Forrestal Building
U.S. Department of Energy
1000 Independence Avenue SW
Washington, DC 20585

Keith Bennett, P.E.
Project Manager
U.S. Department of Energy, Golden Field Office
1617 Cole Blvd
Golden, CO 80401-3393

Karl Bergey
University of Oklahoma
Aerospace Engineering Department
Norman, OK 73069

Mike Bergey
Bergey Wind Power Company
2200 Industrial Blvd.
Norman, Ok 73069

Derek Berry
TPI Composites, Inc.
373 Market Street
Warren, RI 02885-0328

C. P. Sandy Butterfield
NREL/NWTC
1617 Cole Boulevard
Golden, CO 80401

Garrett Bywaters
Northern Power Systems
182 Mad River Park
Waitsfield, VT 05673

Doug Cairns
Montana State University
Department of Mechanical & Industrial Engineering
College of Engineering
P.O. Box 173800
Bozeman, MT 59717-3800

David Calley
Southwest Windpower
1801 West Route 66
Flagstaff, AZ 86001

Stan Calvert
Office of Wind and Hydropower Technologies
EE-2B Forrestal Building
U.S. Department of Energy
1000 Independence Avenue SW
Washington, DC 20585

Jamie Chapman
OEM Development Corporation
840 Summer St.
Boston, MA 02127-1533

Kip Cheney
PO Box 456
Middlebury, CT 06762

Craig Christensen, Vice President
GE Wind
13681 Chantico Road
Tehachapi, CA 93561

R. Nolan Clark
USDA - Agricultural Research Service
P.O. Drawer 10
Bushland, TX 79012

C. Cohee
Foam Matrix, Inc.
1123 E. Redondo Blvd.
Inglewood, CA 90302

Joe Cohen
Princeton Economic Research, Inc.
1700 Rockville Pike
Suite 550
Rockville, MD 20852

C. Jito Coleman
Northern Power Systems
182 Mad River Park
Waitsfield, VT 05673

Ken J. Deering
The Wind Turbine Company
1261 120th Ave. NE
Bellevue, WA 98005

Phillip Dougherty
Office of Wind and Hydropower Technologies
EE-2B Forrestal Building
U.S. Department of Energy
1000 Independence Avenue SW
Washington, DC 20585

S. Finn
GE Global Research
One Research Circle
Niskayuna, NY 12309

Peter Finnegan
GE Global Research
One Research Circle
Niskayuna, NY 12309

R. Gopalakrishnan
GE Wind Energy
GTTC, 300 Garlington Road
Greenville, SC 29602

Dayton Griffin
Global Energy Concepts, LLC
5729 Lakeview Drive NE, Ste. 100
Kirkland, WA 98033

Craig Hansen
Windward Engineering
2225 E. Murray-Holladay Rd. #201A
Salt Lake City, UT 84117

Jim Heath
Entegrity Wind Systems
PO Box 832
Charlottetown, PE C1A 7L9
Canada

Thomas Hermann (5)
Wetzel Engineering, Inc.
P.O. Box 4153
Lawrence, KS 66046-1153

D. Hodges
Georgia Institute of Technology
270 Ferst Drive
Atlanta, GA 30332

William E. Holley
GE Wind Energy
GTTC, M/D 100D
300 Garlington Rd., P.O. Box 648
Greenville, SC 29602-0648

Adam Holman
Alternative Energy Institute
West Texas A & M University
USDA-Agricultural Research Service
Conservation & Production Research Laboratory
P.O. Drawer 10
Bushland, TX 79012-0010

Scott Hughes
NREL/NWTC
1617 Cole Boulevard, MS 3911
Golden, CO 80401

Kevin Jackson
Dynamic Design
123 C Street
Davis, CA 95616

Eric Jacobsen
GE Wind Energy
GTTC, 300 Garlington Road
Greenville, SC 29602

George James
Structures & Dynamics Branch
Mail Code ES2
NASA Johnson Space Center
2101 NASA Rd 1
Houston, TX 77058

Gary Kanaby
Knight & Carver Yacht Center
1313 Bay Marina Drive
National City, CA 91950

M. Kramer
Foam Matrix, Inc.
PO Box 6394
Malibu CA 90264

Alan Laxson
NREL/NWTC
1617 Cole Boulevard
Golden, CO 80401

Bill Leighty
Alaska Applied Sciences, Inc.
P.O. Box 20993
Juneau, AK 99802-0993

Wendy Lin
GE Global Research
One Research Circle
Niskayuna, NY 12309

Steve Lockard
TPI Composites, Inc.
373 Market Street
Warren, RI 02885-0367

James Locke
Wichita State University
207 Wallace Hall, Box 44
Wichita, KS 67260-0044

David Malcolm
Global Energy Concepts, LLC
5729 Lakeview Drive NE, Ste. 100
Kirkland, WA 98033

John F. Mandell
Montana State University
302 Cableigh Hall
Bozeman, MT 59717

Tim McCoy
Global Energy Concepts, LLC
5729 Lakeview Drive NE, Ste. 100
Kirkland, WA 98033

L. McKittrick
Montana State University
Mechanical & Industrial Engineering Dept.
220 Roberts Hall
Bozeman, MT 59717

Amir Mikhail
Clipper Windpower Technology, Inc.
6305 Carpinteria Ave. Suite 300
Carpinteria, CA 93013

Walt Musial
NREL/NWTC
1617 Cole Boulevard
Golden, CO 80401

NWTC Library (5)
NREL/NWTC
1617 Cole Boulevard
Golden, CO 80401

Byron Neal
USDA - Agricultural Research Service
P.O. Drawer 10
Bushland, TX 79012

Steve Nolet
TPI Composites, Inc.
373 Market Street
Warren, RI 02885-0328

Richard Osgood
NREL/NWTC
1617 Cole Boulevard
Golden, CO 80401

Tim Olsen
Tim Olsen Consulting
1428 S. Humboldt St.
Denver, CO 80210

Robert Z. Poore
Global Energy Concepts, LLC
5729 Lakeview Drive NE
Suite 100
Kirkland, WA 98033

Robert Preus
Abundant Renewable Energy
22700 NE Mountain Top Road
Newberg, OR 97132

Jim Richmond
MDEC
3368 Mountain Trail Ave.
Newbury Park, CA 91320

Michael Robinson
NREL/NWTC
1617 Cole Boulevard
Golden, CO 80401

Daniel Sanchez
U.S. Department of Energy
NNSA/SSO
P.O. Box 5400 Mail Stop: 0184
Albuquerque, NM 87185-0184

Scott Schreck
NREL/NWTC
1617 Cole Boulevard
Golden, CO 80401

Brian Smith
NREL/NWTC
1617 Cole Boulevard
Golden, CO 80401

J. Sommer
Molded Fiber Glass Companies/West
9400 Holly Road
Adelanto, CA 92301

Ken Starcher
Alternative Energy Institute
West Texas A & M University
P.O. Box 248
Canyon, TX 79016

Herb Sutherland
1700 Camino Gusto NW
Albuquerque, NM 87107-2615

Andrew Swift
Texas Tech University
Civil Engineering
PO Box 41023
Lubbock, TX 79409-1023

J. Thompson
ATK Composite Structures
PO Box 160433
MS YC14
Clearfield, UT 84016-0433

Robert W. Thresher
NREL/NWTC
1617 Cole Boulevard
Golden, CO 80401

Steve Tsai
Stanford University
Aeronautics & Astronautics
Durand Bldg. Room 381
Stanford, CA 94305-4035

William A. Vachon
W. A. Vachon & Associates
P.O. Box 149
Manchester, MA 01944

Case P. van Dam
Dept. of Mechanical & Aerospace Eng.
University of California, Davis
One Shields Avenue
Davis, CA 95616-5294

Jeroen van Dam
Windward Engineering
NREL/NWTC
1617 Cole Boulevard
Golden, CO 80401

Brian Vick
USDA - Agricultural Research Service
P.O. Drawer 10
Bushland, TX 79012

Kyle Wetzel (5)
Wetzel Engineering, Inc.
PO Box 4153
Lawrence, KS 66046-1153

Mike Zuteck
MDZ Consulting
601 Clear Lake Road
Clear Lake Shores, TX 77565

M.S. 0557	T. J. Baca, 1525
M.S. 0847	J. M. Redmond, 1524
M.S. 0557	T. G. Carne, 1524
M.S. 0557	T. W. Simmermacher, 1524
M.S. 0557	D. T. Griffith, 1524
M.S. 1124	J. R. Zayas, 6333
M.S. 1124	T. D. Ashwill, 6333 (10)
M.S. 1124	D. E. Berg, 6333
M.S. 1124	T. Grisham, 6333
M.S. 1124	P. L. Jones, 6333
M.S. 1124	D. L. Laird, 6333
M.S. 1124	D. W. Lobitz, 6333
M.S. 1124	J. Paquette, 6333
M.S. 1124	M. A. Rumsey, 6333
M.S. 1124	P. S. Veers, 6333
M.S. 0612	A. M. Lucero, 04532
M.S. 0899	Technical Library, 4536 (2)
M.S. 9018	Central Technical Files, 894 4(2)